A&A 507, 131–145 (2009)
DOI: 10.1051/0004-6361/200912177
© ESO 2009

Astronomy & Astrophysics

Large scale structures around radio galaxies at $z \sim 1.5$⋆

A. Galametz[1,2,3], C. De Breuck[1], J. Vernet[1], D. Stern[2], A. Rettura[4], C. Marmo[5], A. Omont[5], M. Allen[3], and N. Seymour[6,7]

[1] European Southern Observatory, Karl-Schwarzschild-Str. 2, 85748 Garching, Germany
e-mail: agalamet@eso.org
[2] Jet Propulsion Laboratory, California Institute of Technology, 4800 Oak Grove Dr., Pasadena, CA 91109, USA
[3] Observatoire Astronomique de Strasbourg, 11 rue de l'Université, 67000 Strasbourg, France
[4] Department of Physics and Astronomy, Johns Hopkins University, 3400 North Charles Street, Baltimore, MD 21218, USA
[5] Institut d'Astrophysique de Paris, CNRS, Université Pierre et Marie Curie, Paris, France
[6] Mullard Space Science Laboratory, UCL, Holmbury St Mary, Dorking, Surrey, RH5 6NT, UK
[7] Spitzer Science Centre, Caltech, 1200 East California Boulevard, Pasadena, CA 91125, USA

Received 25 March 2009 / Accepted 27 August 2009

ABSTRACT

We explore the environments of two radio galaxies at $z \sim 1.5$, 7C 1751+6809 and 7C 1756+6520, using deep optical and near-infrared imaging. Our data cover 15×15 arcmin^2 fields around the radio galaxies. We develop and apply BzK color criteria to select cluster member candidates around the radio galaxies and find no evidence of an overdensity of red galaxies within 2 Mpc of 7C 1751+6809. In contrast, 7C 1756+6520 shows a significant overdensity of red galaxies within 2 Mpc of the radio galaxy, by a factor of 3.1±0.8 relative to the four MUSYC fields. At small separation ($r < 6''$), this radio galaxy also has one $z > 1.4$ evolved galaxy candidate, one $z > 1.4$ star-forming galaxy candidate, and an AGN candidate (at indeterminate redshift). This is suggestive of several close-by companions. Several concentrations of red galaxies are also noticed in the full 7C 1756+6520 field, forming a possible large-scale structure of evolved galaxies with a NW-SE orientation. We construct the color-magnitude diagram of red galaxies found near 7C 1756+6520 ($r < 2$ Mpc), and find a clear red sequence that is truncated at $K_s \sim 21.5$ (AB). We also find an overdensity of mid-infrared selected AGN in the surroundings of 7C 1756+6520. These results are suggestive of a proto-cluster at high redshift.

Key words. large scale structure of Universe – galaxies: clusters: general – Galaxy: evolution – galaxies: individual: 7C 1756+6520 – galaxies: individual: 7C 1751+6809

1. Introduction

Galaxy clusters are the most massive collapsed structures in the universe, which make them an excellent tool for investigating fundamental questions in astronomy. For example, the evolution of cluster number density depends sensitively upon Ω_0, but only weakly upon Λ and the initial power spectrum (e.g., Eke et al. 1998), and thus provides strong constraints on cosmology. Moderate-redshift clusters from well-defined samples such as the *ROSAT* Deep Cluster Survey have been used to constrain Ω_M and σ_8 (Borgani et al. 2001), while Stern et al. (2009) use the ages of cluster ellipticals to constrain the equation of state of dark energy. Distant X-ray luminous clusters provide the best lever arm for such studies, yet few have been found to date. Because galaxy clusters supply large numbers of galaxies at the same redshift, they also provide unique resources to study the formation and evolution of galaxies.

Due to the sensitivity limits of current surveys, it remains challenging to identify a large sample of high redshift galaxy clusters using classical optical and X-ray selection techniques. During the past decade, a new technique for detecting galaxy clusters at $z > 1$ has been to look at the immediate surroundings of high-redshift radio galaxies (HzRGs hereafter; Best et al. 2003; Venemans et al. 2005; Kodama et al. 2007). Indeed, it is now well established that the host galaxies of powerful radio sources are among the most massive galaxies in the universe (Seymour et al. 2007). At low redshift, radio galaxies are associated with giant ellipticals (cD and gE galaxies; Matthews et al. 1964), which are preferentially located in rich environments. Because they are so massive, radio galaxies are excellent signposts to pinpoint the densest regions of the universe out to very high redshifts (e.g., Stern et al. 2003). For example, this has been shown by the strong (5σ) overdensities of Lyα and Hα emitters around HzRGs at $2.1 < z \leq 5.2$ (Kurk et al. 2004a; Miley et al. 2004; Venemans et al. 2005, 2007), believed to be the progenitors of rich, local clusters. However, Lyα and Hα emitters found in these environments are small, faint, blue objects likely to be young star-forming galaxies and probably constitute a small fraction of both the number of cluster galaxies and the total mass of the cluster.

Interestingly, overdensities at the highest redshifts often have a filamentary nature and extend beyond ∼2 Mpc (Croft et al. 2005). Carilli et al. (2002), in a detailed study of filaments in the field of PKS 1138-262, an HzRG at $z = 2.1$, do not detect any extended X-ray emission, indicating that this structure has not yet had sufficient time to virialize. However, Kurk et al. (2004b) show that some segregation has occured, with the Hα emitters, tracing the more evolved population, more centrally concentrated than the younger Lyα emitters. Therefore, the missing link between these proto-clusters and the classical X-ray confirmed clusters found out to $z \sim 1.4$ (e.g., Mullis et al. 2005; Stanford et al. 2006) apparently occurs in the redshift range $1.4 < z \leq 2$.

⋆ Tables 2–6 are only available in electronic form at http://www.aanda.org

Table 1. Observations.

Instrument	Pixel Scale (arcsec/pix)	Band	Wavelength (nm)	Bandwidth (nm)	FoV (arcmin^2)	Exp. Time[a] (min)	Seeing[b] (arcsec)
Palomar/LFC	0.18	*B*	440	100	588/566	345/360	~1
–	–	*z*	900	180	556/442	60/135	~1
CFHT/WIRCAM	0.3	*J*	1252	158	477/482	182/219	0.7–1
–	–	*Ks*	2146	325	477/482	53/64	0.7–1
Spitzer/IRAC	0.61	IRAC1	3560	750	42/42	2/2	1.66
–	–	IRAC2	4520	1010	42/42	2/2	1.72
–	–	IRAC3	5730	1420	42/42	2/2	1.88
–	–	IRAC4	7910	2930	42/42	2/2	1.98

[a] FoV and exposure time for 7C 1751+6809 and 7C 1756+6520 respectively.
[b] Values of the mean *FWHM* for *Spitzer*/IRAC four bands.

This redshift range is therefore particularly interesting for identifying clusters at a redshift beyond where the classical selection techniques are sensitive, but at a redshift where clusters are already partly virialized with a core of older, massive galaxies in place.

In this paper, we present the study of the surroundings of two radio galaxies at $z \sim 1.5$. The next section describes the targets and the multi-wavelength data available for the two fields as well as how we derive the multi-band source catalogs. The third section describes the color criteria we derive to select candidate massive cluster members and the results of this selection. The properties of the cluster member candidates are discussed in Sect. 4. A study of the AGN candidates found in the two fields is also presented in Sect. 5. Section 6 describes possible close-by companions of one of our targeted radio galaxies, 7C 1756+6520. We discuss the results in Sect. 7. We assume a ΛCDM cosmology with $H_0 = 70\,\mathrm{km\,s^{-1}\,Mpc^{-1}}$, $\Omega_\mathrm{m} = 0.3$ and $\Omega_\Lambda = 0.7$. The magnitudes are expressed in the AB photometric system unless stated otherwise.

2. The data

2.1. Target selection

This work follows on the SHzRG project (*Spitzer* High-Redshift Radio Galaxy; Seymour et al. 2007), which was designed to study a representative sample of 70 radio galaxies at $1 < z \leq 5.2$ and their surroundings. SHzRG obtained rest-frame near- to mid-infrared photometry for this sample using all three cameras on board *Spitzer*. From this sample, we selected radio galaxies with $z \sim 1.5$ for further study. From the seven such sources available in the Spring semester of the Northern hemisphere, we selected the two radio galaxies with the most supporting data, 7C 1756+6520 ($z = 1.48$[1]; RA: 17:57:05.44, Dec.: +65:19:53.11) and 7C 1751+6809 ($z = 1.54$; RA: 17:50:49.87, Dec.: +68:08:25.93). These two radio galaxies were first published in Lacy et al. (1992) as part of a sample of 57 radio sources selected at 38 MHz. That paper presents high resolution radio maps of both objects. Their redshifts were first presented in Lacy et al. (1999).

2.2. Observations and data reduction

2.2.1. Palomar/LFC *B*-band data

We imaged the two targets using the Bessel *B*-band filter of the Large Format Camera (LFC; Simcoe et al. 2000) on the Palomar 5 m Hale Telescope (see Table 1). LFC is a prime focus, wide-field optical imager with a well-sampled 24.6 arcmin diameter field, imaged by an array of six 2048 × 4096 pixel backside illuminated SITe CCDs. We observed each target for 6 h in September 2007. The nights were photometric with an average 1″ seeing.

The LFC data were reduced using the `MSCRED` package of IRAF, a suite of tasks designed to process multi-extension, large-format images from the new generation of optical cameras. Processing followed standard optical procedures. A distortion correction was applied to each chip, first using the default solution for LFC, then matching the stars of the USNO-B1.0 catalog (Monet et al. 2003). The final stacked image was therefore astrometrized to the USNO-B1.0 reference frame. For photometry, we calibrated the images using observations of standard stars from Landolt (1992). We then converted to AB magnitudes using: $B_\mathrm{AB} = B_\mathrm{Vega} - 0.1$. We derived the 3σ (5σ) detection limits using 1.5″ diameter apertures uniformly distributed over the images and found limiting magnitudes of ~27.1 (~26.6).

2.2.2. Palomar/LFC *z*-band data

We imaged the radio galaxy fields using the *z*-band filter of Palomar/LFC (see Table 1). In February 2005, we observed 7C 1751+6809 for 60 min under photometric conditions. In August 2005, we observed 7C 1756+6520 for 135 min but in non-photometric conditions. The LFC data were reduced using the `MSCRED` package of IRAF. The standard reduction process included an iterative removal of a *z*-band fringe pattern derived from the supersky flat as well as the same correction of distortion process used for the *B*-band data. The final, stacked images were astrometrically registered to the USNO-B1.0 catalog. The *FWHM* of the final images is ~1.″0 for both fields. Because these data were not all obtained in photometric conditions, nor were these fields covered by the Sloan Digital Sky Survey (SDSS; York et al. 2000), photometric calibration of the *z*-band imaging relied on empirically derived optical through near-IR color relations for Galactic stars. Matching a portion of SDSS imaging data with the Two Micron All Sky Survey (2MASS; Skrutskie et al. 1997), Finlator et al. (2000) show that stars have a well-defined optical/near-infrared color locus, mainly determined by spectral type. We created a 2MASS/SDSS matched catalog of 530 stars with $z < 18$ selected in three random extragalactic fields imaged by both SDSS and 2MASS. Following recent results from the SDSS collaboration[2], SDSS *z* band magnitudes are shifted by 0.02 relative to the AB system in the sense $z_\mathrm{AB} = z_\mathrm{SDSS} + 0.02$. We apply this systematic shift to the SDSS photometry and convert the *J* and

[1] A new spectrum obtained with Keck/Deimos in September 2009 revealed a new redshift $z = 1.416$ for the radio galaxy 7C1756+6520 (based on [NeV]3426, [OII]3727, and [NeIII]3869). This is different from the tentative $z = 1.48$ reported by Lacy et al. (1999), but does not affect the colour selections or conclusions in this paper.

[2] See `http://www.sdss.org/DR2/algorithms/fluxcal.html`.

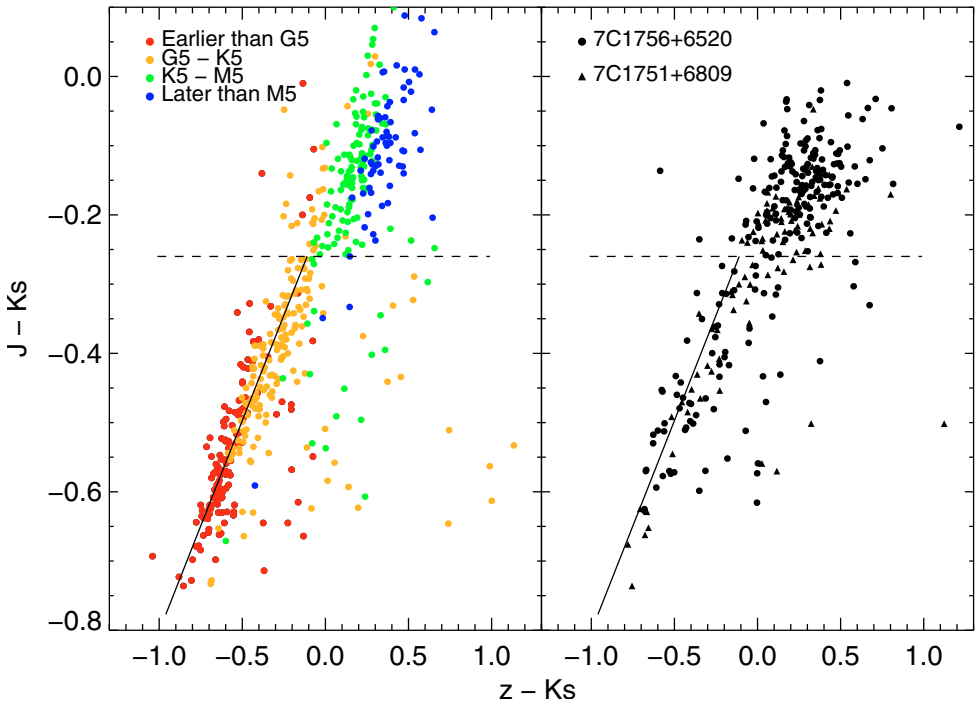

Fig. 1. Color−color diagrams for stars from the matched 2MASS/SDSS catalog (*left*) and for stars in the two radio galaxy fields (*right*). The spectral types of stars in *the left panel* were deduced from optical SDSS colors using Finlator et al. (2000) criteria. As illustrated by the solid line, stars with a spectral type earlier than K5 ($J - Ks < -0.26$) are well fit by an empirical color−color relation, $J - Ks = 0.61(z - Ks) - 0.2$, which was used to calibrate the optical images of the 7C fields using 2MASS stars in each 7C field. The right panel shows the final color−color diagram of the 2MASS stars of our two fields after calibration.

K magnitudes from 2MASS to AB magnitudes using the following corrections: $J_{AB} = J_{Vega}+0.90$ and $K_{AB} = K_{Vega}+1.86$. Using the criteria defined in Finlator et al. (2000) and optical photometry from SDSS (g, r and i-band) to separate stars into spectral classes, we plot their location in a $J - K$ vs. $z - K$ color−color diagram (Fig. 1, left panel). Stars with spectral type K5 and earlier have $J - K < -0.26$ and a color−color relation well fit by a simple linear function: $J - K = 0.61 \times (z - K) - 0.2$. Galaxies and cooler stars have redder $J - K$ colors.

Using 2MASS photometry, we identified stars with a spectral type earlier than K5 in our two radio galaxies fields assuming a $J - K \leq -0.26$ color. We selected 72 and 40 stars, respectively, for 7C 1756+6520 and 7C 1751+6809. Using the above color−color relation, we thus derived the z-band photometric zeropoints for the Palomar data. The color−color diagram for stars in our fields is given in Fig. 1 (right panel). Measuring the dispersion of the empirical color−color relation, we estimate a 0.1 mag uncertainty in the z-band photometric zeropoints. The 3σ (5σ) limiting magnitude determined from random 1.5″ diameter apertures is 25.0 (24.5) for 7C 1756+6520 and 24.8 (24.3) for 7C 1751+6809.

2.2.3. CFHT/WIRCAM data

In order to sample the red side of the 4000 Å break at the redshift of the targets, the radio galaxies fields were observed in the J and Ks bands using the new Wide-field Infrared Camera (WIRCAM; Puget et al. 2004) of the Canada-France-Hawaii Telescope (CFHT; see Table 1). WIRCAM contains four 2048 × 2048 pixel HAWAII2-RG detectors with a gap of 45″ between arrays, and covers a 20′ × 20′ field of view (FoV) with a sampling of 0.3″ per pixel. The imaging observations were obtained in April, May and July 2006 (Projects 06AF38 and 06AF99; P.I. Omont). The seeing varied between 0.7 and 1″ during the observations and the nights were photometric.

The WIRCAM data suffer from serious crosstalk, which echoes all bright objects in the 32 amplifiers of each chip. Although our HzRGs are at high Galactic latitude ($b > 30°$), our images contain numerous bright stars due to the wide field of view of WIRCAM. The crosstalk has different profiles and thus proves especially challenging to correct. Several techniques were attempted to correct crosstalk but none of them were fully satisfactory. For our total exposure time of approximately 3h30 in the J band, the crosstalk is clearly visible for all objects brighter than magnitude 16. In the end, we processed the WIRCAM data without any crosstalk correction and instead flagged the most seriously affected regions (see Sect. 2.3). The remaining processing followed standard near-infrared data reduction strategies. We subtracted the dark and performed flat-fielding with a super flat created from science frames. The images were then sky subtracted and stacked using the reduction pipeline developed by the Terapix team[3] (Marmo 2007). The images were photometrically calibrated to 2MASS J and K bands using ∼60 stars per field. The 3σ (5σ) limiting magnitudes determined from random 1.5″ radius apertures in the J and Ks bands are ∼24.4 (∼23.9) and ∼23.4 (∼22.9), respectively.

2.2.4. Spitzer/IRAC data

Observations with the *Spitzer* Infrared Array Camera (IRAC; Fazio et al. 2004) were performed as part of the GO-1 *Spitzer* program "The Most Massive Galaxies at Every Epoch: a Comprehensive *Spitzer* Survey of High-Redshift Radio Galaxies" (Seymour et al. 2007). These data consisted of four dithered 30 s exposures in each of the four IRAC channels (see

[3] http://terapix.iap.fr

Table 1). The size of the final IRAC mosaic is about $13' \times 7'$. Due to the configuration of the camera, only a $6.5' \times 6.5'$ region is covered with all four bands. The data were processed and mosaiced using the MOPEX package (Makovoz & Khan 2005) from the *Spitzer* Science Center and re-sampled by a factor of two. The final pixel scale is 0.61″ (see Seymour et al. 2007 for further details on the *Spitzer* data and processing). The 5σ limiting magnitudes determined from random 1.5″ radius apertures are 22.1, 21.7, 19.8 and 19.7 for the 3.6, 4.5, 5.8 and 8.0 μm channels, respectively.

2.3. Catalog extraction

For the WIRCAM data, we identified crosstalk-affected pixels in the J band image, the deeper of our WIRCAM bands. A map was created to flag crosstalk contaminated pixels as well as the zones contaminated by bright star artifacts, which accounted for approximately 8% of the final mosaic pixels (see Fig. 2). The J and Ks images were smoothed to the 1″ seeing of the B and z band data. We used SExtractor (Bertin & Arnouts 1996) to extract source catalogs with SExtractor dual mode for J and Ks using the unsmoothed images for object detection and the smoothed one for photometry. For B, z, J and Ks bands, we derived colors using a fixed 2.″5 diameter aperture. For total magnitudes, we used the Kron automatic aperture photometry given by the SExtractor MAG_AUTO parameter. All magnitudes were corrected for Galactic extinction using the dust maps of Schlegel et al. (1998) assuming the $R_V = A_V/E(B-V) = 3.1$ extinction law of Cardelli et al. (1989). Since both fields are at high Galactic latitude, their extinction maps are very uniform. For both fields, the applied corrections were 0.18 in B-band, 0.06 in z, 0.04 in J and 0.02 in Ks.

The point source function (PSF) of IRAC is well defined (Lacy et al. 2005), providing consistent and readily tabulated aperture corrections to determine total magnitudes from aperture photometry. For both magnitudes and colors, we chose an aperture of 2″5 diameter and corrected the measured flux by the corresponding multiplicative correction factors – i.e., 1.68, 1.81, 2.04 and 2.45 for the 3.6, 4.5, 5.8 and 8.0 μm channels, respectively.

Combining all of these catalogs, we built a master catalog which provides multiwavelength data for all sources detected in at least one of the eight bands observed. The final surface covered by B, z, J and Ks and not affected by the WIRCAM cross-talk is ~0.1 square degrees. Figure 3 shows the galaxy number counts for the different bands compared with previous counts from the literature. The galaxies were first isolated from the stars based on SExtractor parameter CLASS_STAR. The 1σ error on the number counts is overplotted in Fig. 3, assuming a Poisonnian error. No incompleteness correction was applied to the counts.

The galaxy counts determined from B, J and Ks were compared to previous works: Williams et al. (1996); Metcalfe et al. (1995, 1991) for B, Maihara et al. (2001); Teplitz et al. (1999) for J and Elston et al. (2006); Maihara et al. (2001) for Ks. For the z-band, we derive number counts from zBoötes (Cool 2007), a z-band survey of the Boötes field that covers 7.62 square degrees and reaches a 50% completeness limit of 23.4[4]. We also derive z-band number counts from the GOODS-MUSIC catalog, a multiwavelength catalog of *Chandra* Deep Field South (CDFS) in the GOODS South field (Grazian et al. 2006b, see Sect. 3.1 for details on this catalog).

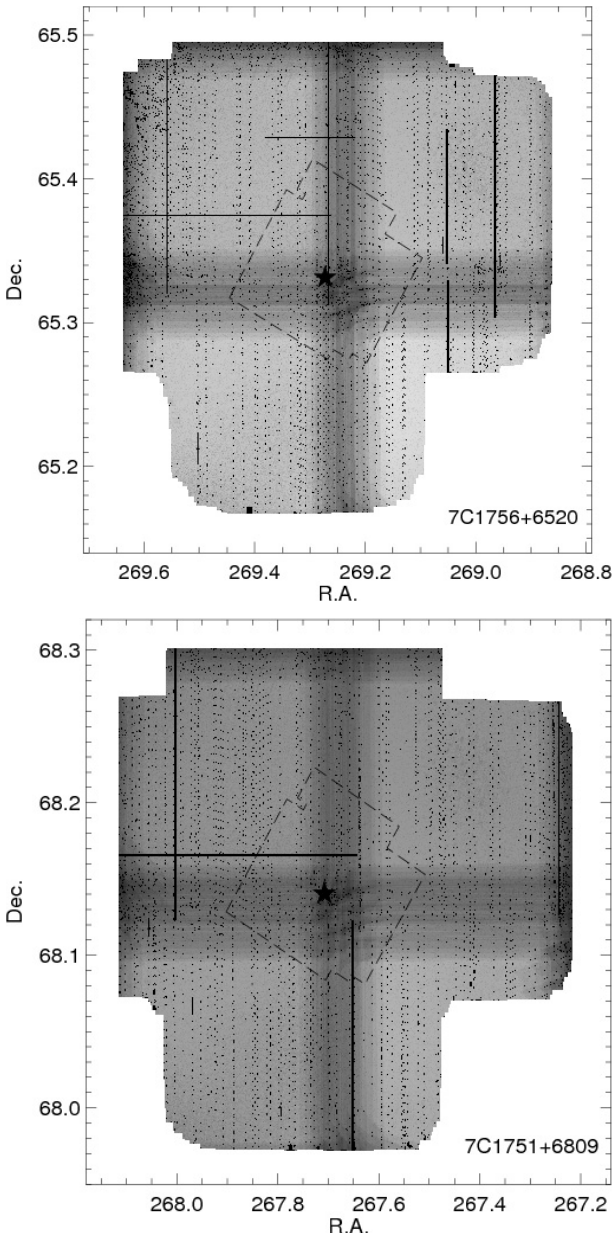

Fig. 2. Combined field covered by our B, z, J and Ks-band data showing both the weight map of the WIRCAM data (J) and the cross-talk flag map. We also flag regions contaminated by bright stars. The dashed lines outline the regions covered by the four IRAC bands. The positions of the HzRGs in the fields are indicated by stars.

The B, z and J-band counts are found in good agreement with the literature. The Ks-band counts are also found in agreement with previous studies for the field around 7C 1751+6809. The field around 7C 1756+6520 however shows an excess of sources with $17 < Ks < 20.5$; at the faint limit, Ks number counts drop due to incompleteness. This overdensity is the first evidence of an overdensity of very red objects around this radio galaxy.

2.4. Completeness

In order to assess the completeness limit of our images, artificial galaxies of different types were added to our images using the IRAF `artdata` package (`gallist` and `mkobjects` routines).

[4] The final catalogs and images are available at `http://archive.noao.edu/nsa/zbootes.html`.

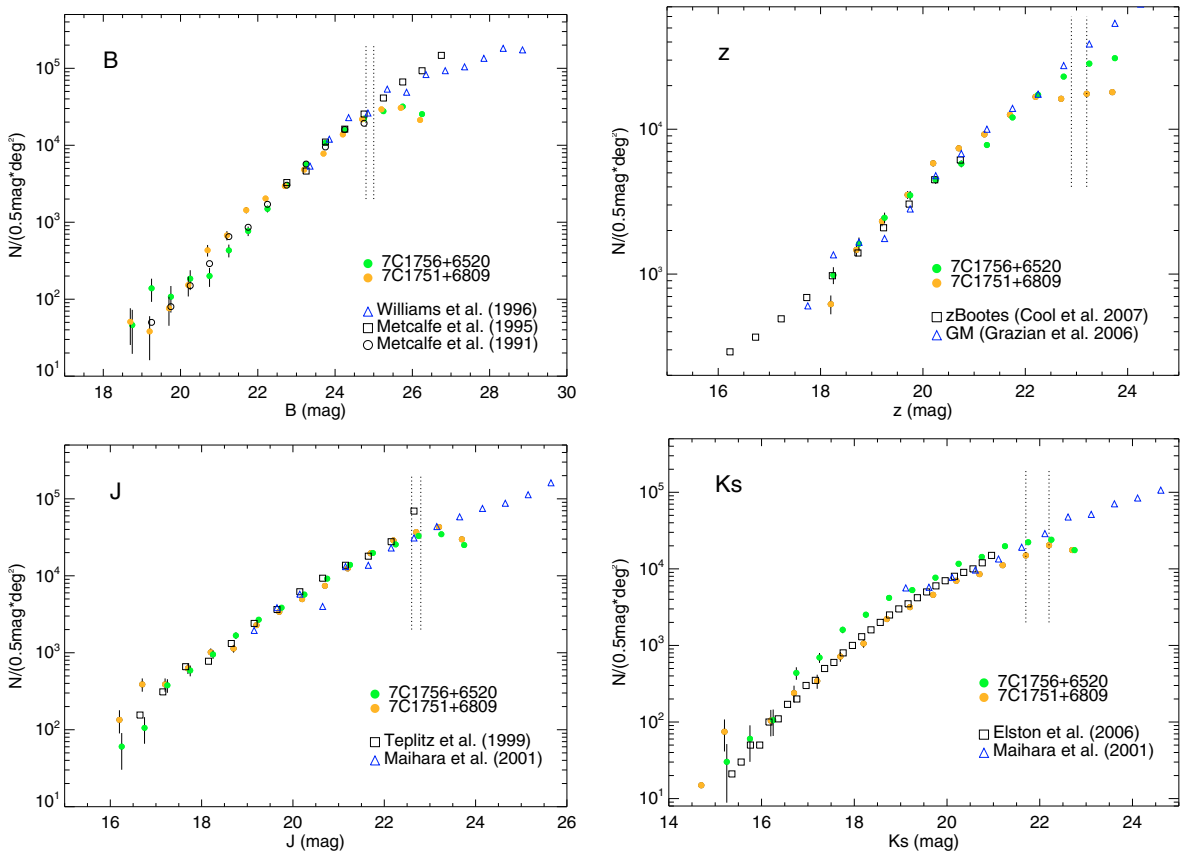

Fig. 3. Galaxy number counts for our B, z, J and Ks data. We use the stellar index determined by SExtractor (CLASS_STAR) to separate galaxies from stars. No completeness correction was applied. The 90% completeness limits of our images for elliptical and spiral galaxies are indicated by the two vertical dotted lines. We plot number counts from the literature (see legends for symbols; GM: GOODS-MUSIC). The counts in B, z and J are found in good agreement with the literature. However, the 7C 1756+6520 field shows an excess of sources with $17 < K\text{s} < 20.5$, the first evidence of an overdensity of very red objects in this field.

We first consider the completeness limit for elliptical galaxies. For half magnitude intervals of brightness, we created catalogs of 5000 elliptical galaxies which were randomly added to the B, z, J and Ks images, including Poisson noise. We adopted a de Vaucouleurs surface brightness law, a minimum galaxy axial ratio b/a of 0.8 and a maximum half flux radius of 1.″0. Running SExtractor with the same configuration files used for the unadulterated data, we determined the fraction of artificial sources detected. For ellipticals, the derived 90% completeness limits for our images are 25.0, 23.2, 22.8, and 22.2 in the B, z, J and Ks bands, respectively. We then determined the completeness limit for spiral galaxies by creating catalogs of 5000 spirals galaxies assuming an exponential disk surface brightness law with a minimum b/a of 0.8 and a maximum half flux radius of 1.″0. The derived 90% completeness limits are 24.8, 22.9, 22.6 and 21.7 in the B, z, J and Ks bands, respectively. As expected, the completeness limit for exponential profile galaxies is slightly worse than for ellipticals due to the less compact nature of their morphologies.

3. Candidate massive cluster members at $z \sim 1.5$

We now consider the environments of 7C 1756+6520 and 7C 1751+6809. We first introduce a color criterion to select candidate cluster members based on the BzK selection technique of Daddi et al. (2004). We then discuss the selection of candidates selected using the full multiwavelength master catalog (Sect. 2.3) and finally present the results on the properties and clustering of these sources.

3.1. Color selection of evolved galaxies at $z \sim 1.5$

Substantial effort has gone into identifying color criteria to select galaxies and galaxy cluster members at high redshift. Selecting extremely red objects (EROs; $R - K \geq 4$), Stern et al. (2003) and Best et al. (2003) successfully identified evolved galaxy overdensities around HzRGs at $z \approx 1.1{-}1.6$. It has been shown that near-IR color criteria can be used to robustly identify passively evolving galaxies at $z \gtrsim 2$. These criteria are mainly based on the position of the 4000 Å break at a given redshift. Thus, the criterion $(J - K\text{s})_{\text{Vega}} > 2.3$, which was first exploited by the FIRES team (Franx et al. 2003), is now well established and has been used to select cluster members at $z > 2$ (Distant Red Galaxies, hereafter DRGs; Kajisawa et al. 2006; Tanaka et al. 2007). The galaxies selected by this criterion are mainly massive, evolved galaxies with old stellar populations. The goal of the current study is devise color criteria that are optimized for identifying evolved galaxies at $z \gtrsim 1.4$, sampling slightly higher redshifts than the ERO selection criteria, but not as high redshift as the DRG or Lyman break selection criteria.

Based on the K20 survey (Cimatti et al. 2002), Daddi et al. (2004) proposed a simple two-color criterion based on BzK-band photometry for identifying galaxies at $1.4 \leq z \leq 2.5$ and classifying them as either star-forming galaxies, selected by $BzK \equiv (z - K) - (B - z) > -0.2$ (hereafter sBzK galaxies) or passive

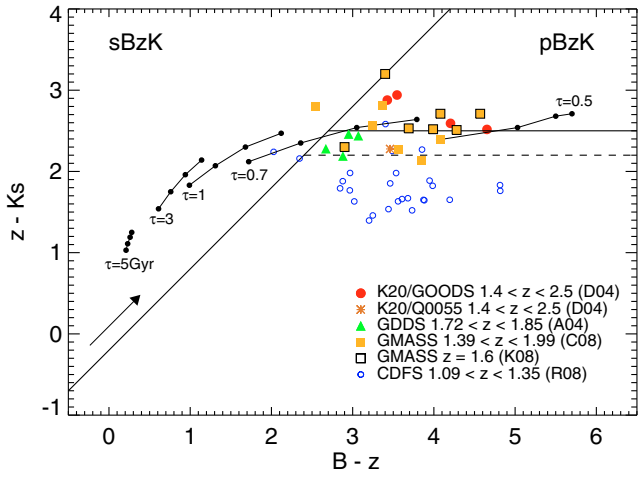

Fig. 4. BzK color−color plot of stellar population models at $z = 1.5$. The curves account for star formation histories with various τ models (respectively from left to right $\tau = 5, 3, 1, 0.7$ and 0.5 Gyr). For each model, black points indicate four different ages of the population ($t = 2.5, 3, 3.5$ and 4 Gyr). The black arrow indicates a dust extinction of $E(B-V) = 0.2$ as parameterized with the reddening curve of Cardelli et al. (1989). The models are consistent with the BzK criteria of Daddi et al. (2004; solid lines). However, the BzK color selection for pBzK galaxies is relatively strict and omits some passive elliptical galaxies at $z \sim 1.5$. We plot the early-type galaxies with a spectroscopic redshift $1.4 < z < 2.5$ found in the literature (K20 – Daddi et al. 2004 – D04; GDDS – Abraham et al. 2004 - A04; GMASS – Cimatti et al. 2008 – C08; Kurk et al. 2008 – K08). We revise the pBzK criterion and adopt $z-Ks > 2.2 \cap BzK < -0.2$ to select passive candidates at $z > 1.4$ (dashed line). This criterion has been chosen as a compromise between selecting the majority of the passive galaxies candidates and avoiding contamination by lower redshift red objects. Contamination is expected to be small, though, as shown by the location of a sample of spectroscopically confirmed elliptical galaxies at lower redshift ($1.09 < z < 1.35$ – CDFS – Rettura et al. 2008 – R08) with only 15% of them selected by our extended BzK criteria.

evolving systems, selected by $BzK < -0.2 \cap (z-K) > 2.5$ (hereafter pBzK galaxies). The BzK selection is largely insensitive to dust extinction since $E(B-V)$ is parallel to $BzK = -0.2$ criterion (Daddi et al. 2004). This two-color selection is therefore particularly efficient at isolating the red massive component of galaxy clusters at $z \geq 1.4$.

We consider first the colors of different stellar populations at $z \sim 1.5$ obtained from the Bruzual & Charlot (2003) models (Fig. 4). The different curves show the various dust-free τ models predictions (from left to right, $\tau = 5, 3, 1, 0.7, 0.5$ Gyr), assuming solar metallicity and a Salpeter (1955) initial mass function. For each model, four different population ages are indicated ($t = 2.5, 3, 3.5$ and 4 Gyr). As previously stated, the BzK criterion is relatively insensitive to dust extinction since the reddening vector for an extinction of $E(B-V) = 0.2$ is almost parallel to the $BzK = -0.2$ line (see black arrow in Fig. 4).

The model colors are consistent with the BzK selection criterion, with models covering first the sBzK zone and then the pBzK zone of the BzK diagram as τ decreases. We note however that the criterion is most likely missing early-type galaxies at $z > 1.4$, in particular those with the youngest stellar populations (models with small τ and large t values). We overplot a sample of the (rare) examples of early-type galaxies at $1.4 < z < 2$ and spectroscopically confirmed in the literature. Daddi et al. (2004) report five high redshift early-type galaxies from the K20 survey, classified as such on the basis of continuum breaks and absorption lines in their spectra. Four are in the GOODS area and one is in the Q0055 area. Cimatti et al. (2008) used the Galaxy Mass Assembly ultra-deep Spectroscopic Survey (GMASS; Kurk et al. 2008) to find passive galaxies at $z > 1.4$. They used the UV properties of passive galaxies and derived a color index of the UV continuum for galaxies with spectroscopic redshift $z > 1$ (see Cimatti et al. 2008, for details). Thirteen passively evolving galaxies at $1.390 < z < 1.981$ were found in GMASS, seven of which are members of an overdensity at $z \sim 1.6$ (Kurk et al. 2008). The Gemini Deep Deep Survey (GDDS; Abraham et al. 2004) obtained spectroscopy for 309 objects attempting to target galaxies in the "redshift desert" ($1 < z < 2$)[4]. Fifty of these sources have BzK photometry (SA12 and SA15 fields) and $z \geq 1.4$, of which five have $BzK < -0.2$. One of these sources is at $z > 2$ and has a $z - K$ which is far too blue to be considered as a passively evolving galaxy ($z - K < 1$). We therefore find only four strong candidates for passively evolving galaxies in GDDS. The location of all these passive galaxies in the BzK diagram is given in Fig. 4. Nine out of 22 are found to have $z - K < 2.5$. We thus confirm what we had already suspected from the models, i.e. the BzK criterion for the pBzK selection is missing a significant fraction (~40%) of old galaxies at $z > 1.4$.

We revise the pBzK criterion and adopt $z - Ks > 2.2$ rather than $z - Ks > 2.5$, coupled with $BzK < -0.2$, to select passively evolving galaxies at $z > 1.4$ (hereafter pBzK* galaxies). This color cut has been chosen as a compromise between following the elliptical model color predictions as well as selecting the majority (91%) of spectroscopically confirmed passive systems at $z > 1.4$ to date and minimizing contamination from very red galaxies at lower redshift. Rettura et al. (2008) study a sample of 27 early-type galaxies found in the CDFS with $1.09 < z < 1.35$. Out of 27, only four (all with $z > 1.3$) are selected with our extended BzK criteria (see Fig. 4, open circles; BzK photometry from A.Rettura, private communication). We are therefore confident that the contamination of lower redshift red objects is small. Indeed, since the 4000 Å break is at the red end of the z-band at $z \sim 1.4$, the $z-Ks$ color increases rapidly with redshift for $z \sim 1.4$ making this simple color criteria an efficient redshift indicator, especially for passive systems.

Grazian et al. (2006b) presents the GOODS MUlticolor Southern Infrared Catalog (GOODS-MUSIC), a multiwavelength catalog of the GOODS South field, combining imaging ACS (optical), VLT (near-infrared), and *Spitzer* (mid-infrared) data with available spectroscopic data. Grazian et al. (2006b) applied a photometric redshift code to this multiwavelength dataset[5]. For this study, we used an updated version of the GOODS-MUSIC catalog (version 2) recently presented in Santini et al. (2009). The new catalog contains, among other things, additional spectroscopic redshifts and new MIPS 24 μm photometry. The total area covered by the GOODS-MUSIC catalog is 143.2 square arcmin. We check the revised BzK selection technique using the photometric redshifts ($z_{\rm phot}$ hereafter) of the pBzK (65), pBzK* (116) and sBzK (4727) galaxies found in the GOODS-MUSIC catalog. Of the pBzK galaxies, 56% (78%) are found with $z_{\rm phot} > 1.4$ ($z_{\rm phot} > 1.2$). The corresponding percentages are 49% (74%) for the pBzK* galaxies and 82% (88%) of

[4] The GDDS catalog is publicly available at http://lcirs.ociw.edu/public/GDDSSummary-dist.txt. Targeted magnitudes are in the Vega system. We convert from Vega to the AB photometric system using the corrections adopted earlier in this paper.

[5] The full catalog, including photometric redshifts, is publicly available at http://lbc.mporzio.astro.it/goods/goods.php.

the sBzK galaxies. Using the same photometric redshift code as used for GOODS-MUSIC $z_{\rm phot}$, Grazian et al. (2006a) estimate an accuracy of $\sigma_z = 0.05 \times (1+z)$ for red galaxies ($J-K > 0.7$) and $\sigma_z = 0.03 \times (1+z)$ for their full sample. Figure 2 of the same paper shows that, at all redshifts, the photometric redshifts systematically underestimate the spectroscopic redshifts. Similar results were also found in Mobasher et al. (2004) whose photometric redshifts in the GOODS Southern Field at $z > 1.3$ were also underestimated. The percentages presented above are thus likely lower limits. The revised BzK selection is therefore very efficient at isolating red galaxies at $z > 1.4$, with some inevitable contamination by lower redshift reddened galaxies.

3.2. Candidate cluster members

The combination of filters used during the observations were checked for consistency with the one used by Daddi et al. (2004). Comparing the shape of the filter transmission curves, we deduce that the B-band filters are equivalent. The z-band filter of Palomar/LFC is consistent with the Gunn z-band of VLT/FORS1 though it is shorter at long wavelength by ~400 Å. Finally, the CFHT/WIRCAM Ks-band filter is slightly more extended at bluer wavelength (by ~300 Å) compared to the one used at VLT/ISAAC by Daddi et al. (2004). We use a library of galaxy templates generated with PÉGASE2 (Projet d'Étude des Galaxies par Synthèse Évolutive; Fioc & Rocca Volmerange 1997) and compare the colors obtained with the different filter sets. We conclude that the correction to the $B-z$ color is negligible, especially for galaxies at intermediate to high redshift ($z \geq 1.4$ – less than 0.02) and the correction to $z-Ks$ color is not systematic (i.e., depending on the galaxy type and age) and are generally smaller than the calibration error of our z-band photometry (e.g. ≤0.1 mag on average; see Sect. 2.2.2).

We next verify that the depth of our data is sufficient to select passively evolving systems at $z > 1.4$. The magnitudes of early-type galaxies at $z > 1.4$ and confirmed spectroscopically are, unfortunately, rarely given in the literature. Furthermore, the selection of such objects itself is strongly biased to the brightest objects. We look at the expected magnitudes of pBzK* galaxies in the GOODS-MUSIC catalog (see §3.1). 57 objects have $z_{\rm phot} > 1.4$ and BzK magnitudes fitting the pBzK* criteria (hereafter the "GM sample"). These sources have $24.8 < B < 29.7$ ($\langle B \rangle \sim 28.2$), $22.2 < z < 26.2$ ($\langle z \rangle \sim 24.4$) and $19.7 < Ks < 24.4$ ($\langle Ks \rangle \sim 21.8$). Considering the 3σ limits of our imaging, our Ks data would detect 98% of the GM sample, our z data would detect 75% of the GM sample, but our B data would detect only 11% of the GM sample. Therefore, we treat the z-band as the limiting band for this work and consider sources with upper limits in B. However, at a given B magnitude, fainter objects in z will have a bluer $B-z$ color, corresponding to bluer objects. We are therefore confident that the majority of very red passive members of the clusters will be selected in our dataset.

We select the sBzK, pBzK and pBzK* galaxies around 7C 1756+6520 and 7C 1751+6809 using our multi-wavelength catalog. The coordinates and B, z, J and Ks magnitudes of the pBzK* galaxies are given in Tables 5 and 6 for 7C 1756+6520 and 7C 1751+6809 respectively. We assume Poisson errors for source density determinations. Figure 5 shows the BzK color diagram of all the objects with a 3σ detection in B, z and Ks. We also plot the sources that have a $z-Ks > 2.2$ but no (or $<3\sigma$) detection in the B-band (arrows). In order to place those sources in Fig. 5, we assign them the 3σ detection limit for the B magnitude ($B = 27.1$). For 7C 1756+6520 (7C 1751+6809), we found 129 (106) pBzK* galaxies including 42 (42) pBzK galaxies (with a 3σ detection in z and Ks). This gives a surface density of 0.39 ± 0.03 (0.32 ± 0.03) arcmin^{-2} for pBzK* galaxies and 0.13 ± 0.02 (0.12 ± 0.02) arcmin^{-2} for pBzK galaxies. We extract the star-forming candidates with a 3σ detection in B, z and Ks and found 218 (200) sBzK galaxies, i.e., a surface density of 0.65 ± 0.05 (0.59 ± 0.04) arcmin^{-2}. 14 (26) sources have $z-Ks > 2.2$ and no (or $<3\sigma$) detection in B (green arrows) and can not be reliably distinguished as star-forming or passive systems.

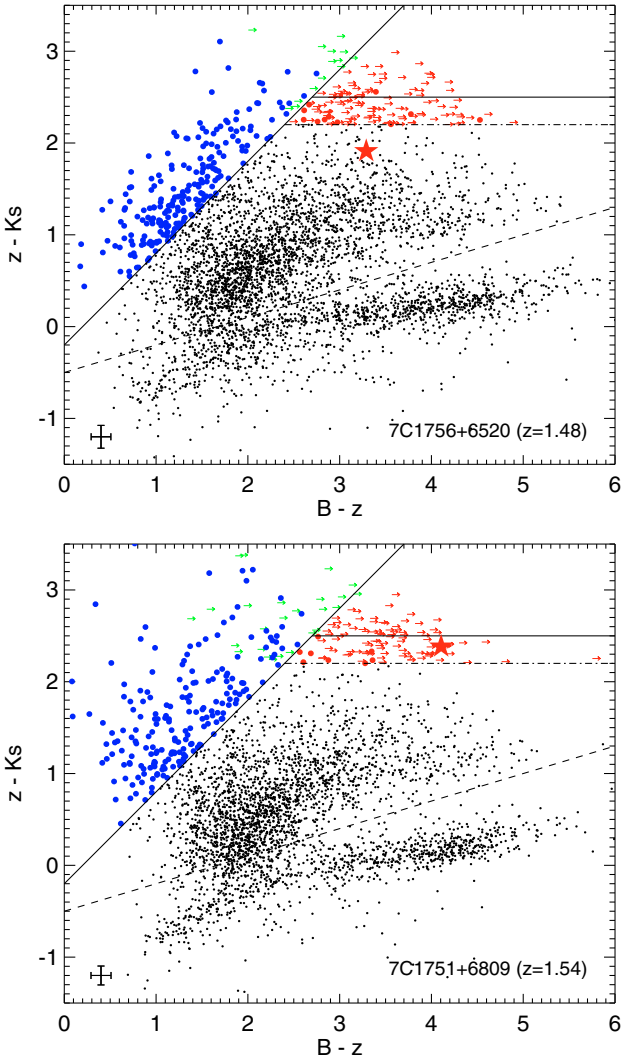

Fig. 5. Color–color BzK diagram of 7C 1756+6520 at $z = 1.48$ (*top*) and 7C 1751+6809 at $z = 1.54$ (*bottom*). The sBzK and pBzK selection regions defined by Daddi et al. (2004) are shown by the solid lines. Our new pBzK* selection is shown by the dot-dashed line. The dashed line separates stars and galaxies. All sources with a 3σ detection in B, z and Ks are plotted. Also plotted are the sources with a $z-Ks > 2.2$ but no (or $<3\sigma$) detection in the B-band (arrows). In order to place those sources in the plot, we assign them the 3σ detection limit for the B magnitude ($B = 27.1$). Typical uncertainties on colors are indicated in *the lower left corner* of each plot. HzRGs are marked as red stars (7C 1751+6809 has only an upper limit in the B-band).

Considering the $J-Ks$ color of the BzK sources, there is a clear difference between sBzK and pBzK galaxies, with pBzK galaxies having a redder and narrower distribution centered around $\langle J-Ks \rangle \simeq 1.07$ (0.93) for the 7C 1756+6520

(7C 1751+6809) field. sBzK galaxies have a $\langle J - Ks \rangle \simeq 0.71$ (0.57). We note that the pBzK* galaxies found around 7C 1756+6520 are, on average, redder that those found in the 7C 1751+6809 field.

3.3. Surface density of BzK-selected galaxies

We now compare the densities found in our HzRG fields to blank fields. Grazian et al. (2007) study the properties of various classes of high redshift galaxies, including pBzK and sBzK sample in the GOODS-MUSIC sample. They compare their number densities of sBzK and pBzK galaxies with the literature (Daddi et al. 2004; Kong et al. 2006; Reddy et al. 2006) and conclude that the GOODS-South field is representative of the distant universe. We therefore use the GOODS-South as a first comparison field for our HzRG field. We cut the GOODS-MUSIC catalog at the same completeness limit as our data, i.e., we select pBzK and pBzK* galaxies to our 90% completeness limits of $Ks < 22.2$ and $z < 23.2$, and we select sBzK galaxies to $Ks < 21.7$ and $z < 22.9$. The number densities of sBzK, pBzK and pBzK* galaxies in the GOODS-MUSIC catalog are given in Table 2 (Col. 2) assuming Poisson errors on the numbers. The corresponding densities in our two fields (corrected for incompleteness) are given in Cols. 8 and 10.

We also compare our results to the MUSYC survey. The MUSYC survey (Gawiser et al. 2006; Quadri et al. 2007) consists of four fields: an extended Hubble Deep Field South (E-HDFS), an extended Chandra Deep Field South (E-CDFS) and two fields called SDSS 1030 and CW 1255. We note that the region covered by GOODS-MUSIC is included in the E-CDFS. Optical and near-infrared imaging of $30' \times 30'$ were obtained for all the fields. Deeper near-infared imaging of $10' \times 10'$ were obtained for subfields of SDSS 1030 and CW 1255 as well as for two adjacent subfields of E-HDFS (resulting in a deeper subfield of $20' \times 10'$ for E-HDFS). The MUSYC team did not obtain additional data for E-CDFS since the region had already been observed extensively by the GOODS team. All images and photometric catalogs are available on the MUSYC website[5]. We use four *UBVRIzJHK* catalogs of the MUSYC fields i.e., the multiwavelength catalogs of the deepest subfields in E-HDFS (201.1 sq. arcmin), SDSS 1030 (106.7 sq. arcmin) and CW 1255 (101.9 sq. arcmin) presented in Quadri et al. (2007) and the catalog of the full E-CDFS (969.6 sq. arcmin; Taylor et al. 2009 in preparation). For each field, we select the pBzK, pBzK* and sBzK galaxies to the 90% completeness limit of our data. Surface densities of the MUSYC fields are given in Table 2 (Cols. 3–6). The surface densities derived from the four MUSYC fields is given in Col. 7. Since GOODS-MUSIC is in E-CDFS, the surface densities for those two fields are not independent; see Table 2, Cols. 2, 3.

Whereas the star-forming sBzK galaxies only vary by up to 70% from field to field, the red pBzK and pBzK* galaxies show significant field to field variations. The surface densities of both pBzK and pBzK* galaxies around 7C 1756+6520 are comparable to the MUSYC SDSS 1030 field, the denser control field as far as the red galaxies are concerned. We find an excess of pBzK and pBzK* galaxies by a factor of 2.4 ± 1.2 and 1.7 ± 0.4 relative to the average density derived from the four MUSYC fields. The density of sBzK in the full 7C 1756+6520 field is, on the contrary consistent with the control fields. We find that BzK densities in 7C 1751+6809 are all in good agreement with MUSYC and GOODS-MUSIC.

[5] http://www.astro.yale.edu/MUSYC/

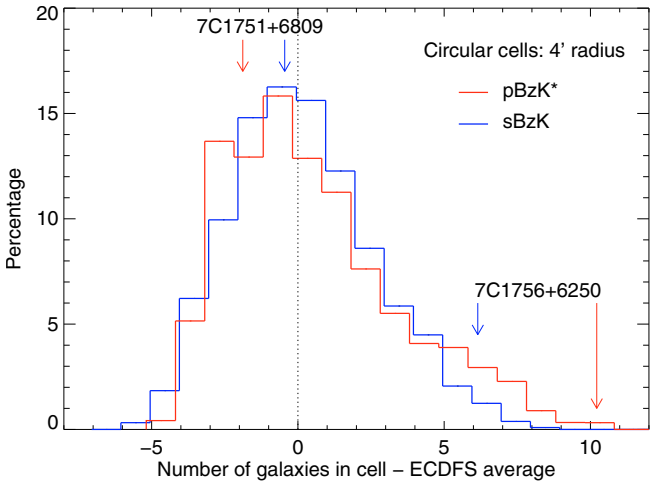

Fig. 6. Histogram of the number of pBzK* (red) and sBzK (blue) galaxies in the MUSYC E-CDFS field in circular cells of 4′ radius (equivalent to 2 Mpc at $z = 1.48$). We subtract from our counts the number of galaxies expected in such a cell corresponding to the E-CDFS average density (7.05 for sBzK and 5.18 for pBzK*). Cells below (above) 0 are therefore underdense (overdense) compared to the full field. Arrows indicate the number of galaxies found within 2 Mpc of our two HzRGs. We first note that the tail of the red galaxies distribution falls further than the blue galaxies one, confirming that red galaxies are more clustered than blue ones. 7C 1751+6809 is found in a slightly underdense region for both blue and red BzK. The number of pBzK* for 7C 1756+6520 falls at the very end of the tail of the distribution with only 0.26% of the cells containing such a high number of red objects.

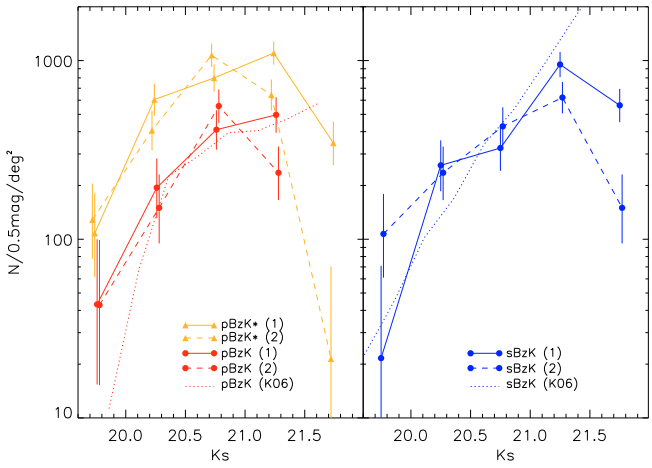

Fig. 7. Ks number counts for pBzK (red), pBzK* (orange) and sBzK galaxies (blue) compared with counts from Kong et al. (2006; K06). The solid and dashed lines correspond to 7C 1756+6520 (1) and 7C 1751+6809 (2), respectively.

Overdensities of narrow-band emitters and EROs have been found out to 1.75–2 Mpc in protoclusters around HzRGs at $2 < z < 3$ (Kurk et al. 2004b; Venemans et al. 2007). Best et al. (2003) studied the radial distribution of EROs around powerful radio-loud AGN at lower redshifts ($z \sim 1.6$) and found overdensities on scales of at least 1 Mpc for four fields out of the six in their sample. We therefore also compute the density of sources found within 2 Mpc (~4′) of the radio galaxies (Table 2, Cols. 9 and 11). The corresponding region is also outlined by dashed lines in Fig. 8. No excess of BzK galaxies is found in the close surroundings of 7C 1751+6809. This region is actually under-dense for elliptical candidates by a factor of two compared

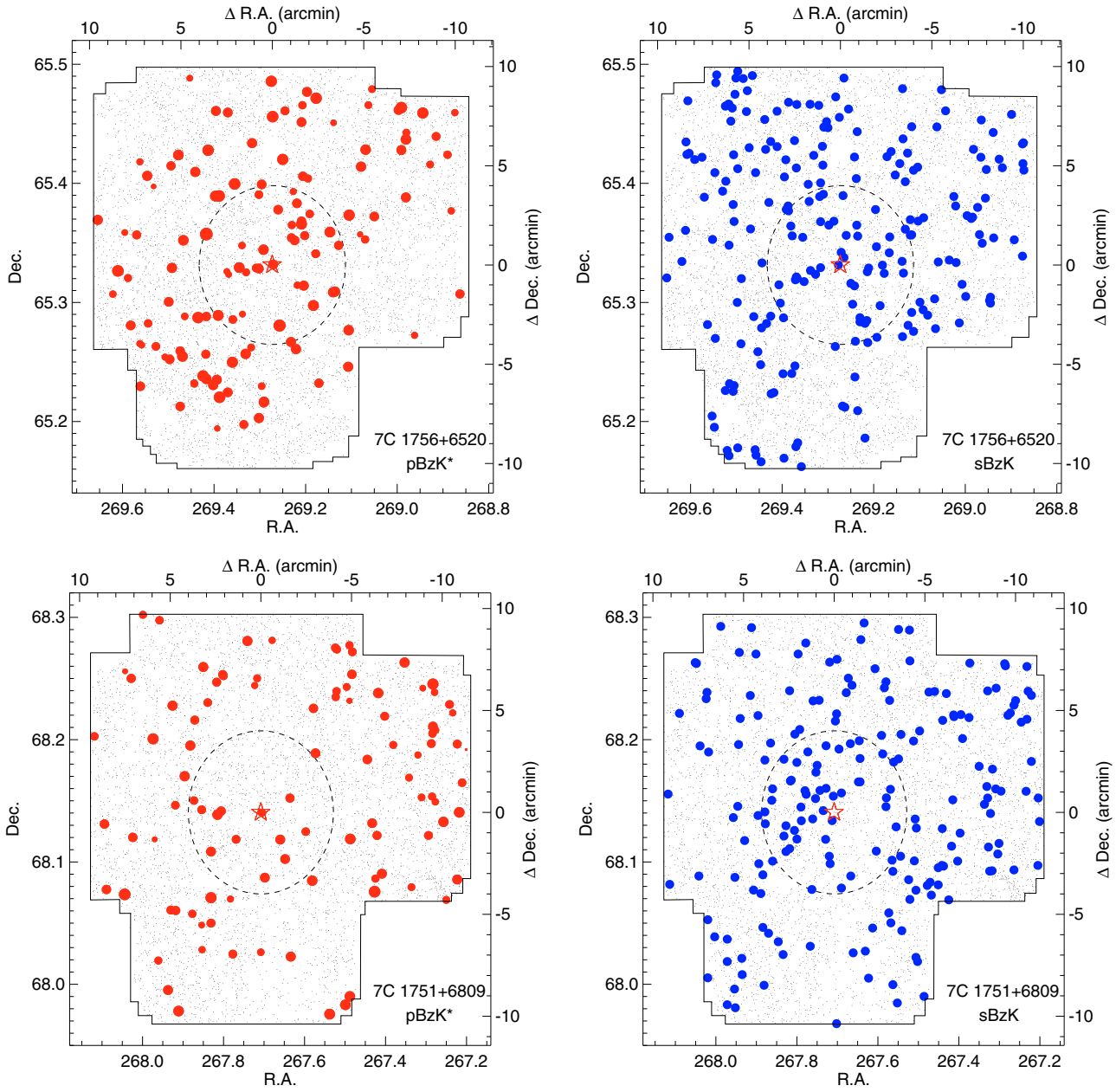

Fig. 8. Spatial distribution of the *BzK*-selected galaxies in the two fields: *left panels*, p*BzK** galaxies in red with the size of the symbol scaled according to the *K*s-magnitude; *right panels*, s*BzK* galaxies in blue. The radio galaxies are marked by the red stars. The area simultaneously covered by the *BzK* bands is outlined and all sources detected in all three bands (3σ) are indicated by black points. The coordinates are also given relative to the radio galaxy in arcmin (*right and top axes*). The 2 Mpc radius region around the HzRG is marked by the dashed line.

to the full field. A concentration of galaxies is found in the 2 Mpc surroundings of 7C 1756+6520 for p*BzK*, p*BzK** and s*BzK* galaxies not only compared to the control fields (by a factor of 4.7 ± 2.4, 3.1 ± 0.8 and 2.0 ± 0.6 respectively) but also compared to the full 7C 1756+6520 field (by a factor of 1.7 ± 0.9, 1.9 ± 0.5 and 2.0 ± 0.6 respectively). We note that the full field 7C 1756-6520 is biased towards higher densities since it contains the excess of sources near the HzRG. If we compute the surface density of p*BzK** in the rest of the field removing the 2 Mpc surroundings of the HzRG, the surface density reduces to 480 ± 80 sources per sq. degrees implying that the inner 2 Mpc region is denser by a factor of 2.4 ± 0.7 compared to the rest of the field.

In order to further quantify the probability to find an overdensity of p*BzK** and s*BzK* galaxies in a 2 Mpc radius region, we now work out the counts-in-cells fluctuations of E-CDFS, the largest field of MUSYC. We measure the number of p*BzK** and s*BzK* galaxies (in the limits of completeness) found in 10 000 randomly placed circular cells of 4′ radius (corresponding to 2 Mpc radius at $z = 1.48$) in the E-CDFS 969.6 sq. arcmin field of view. Edges were avoided by forcing the cells centers to be at least 4′ distant from the edges of the E-CDFS field. We chose a large number of cells (allowing some overlapping) to fully sample the counts fluctuations. We do not consider counts-in-cell of p*BzK* in this analysis due to the very small number of these galaxies in E-CDFS (18). Figure 6 shows the histogram of counts-in-cells. s*BzK* are more common than p*BzK**. In order to be able to directly compare those two populations, we subtract from our counts the expected average density in E-CDFS scaled to the cell size. Counts are given in percentage of the total

number of cells. We also mark with arrows the galaxies counts within 2 Mpc of our two HzRGs (also corrected from the average E-CDFS density). The histogram has a right-skewed distribution. We note that the tail of the distribution of red galaxies is longer that the one for blue galaxies confirming that red galaxies are more clustered than blue ones (see Daddi et al. 2000; Kong et al. 2006). Counts in 7C 1751+6908 are consistent, if anything slightly lower, than the average of E-CDFS. The counts of pBzK* and sBzK galaxies around 7C 1756+6520 on the contrary fall way beyond the average density in E-CDFS, near the end of the tail of the distribution with only 0.26% of the cells having similar densities, confirming the result that the HzRG is found in an exceptionally overdense region.

3.4. Number counts

We derive the Ks-band number counts in 0.5 mag bins for pBzK, pBzK* and sBzK galaxies in our two fields (Fig. 7). We adopt Poissonian errors for the counts and use the Gehrels (1986) small numbers approximation for Poisson distributions. We overplot the findings of Kong et al. (2006; K06 hereafter) as a dotted line for comparison (see also Lane et al. 2007; Imai et al. 2008; Hartley et al. 2008). The number counts become incomplete at Ks > 21 when we start reaching the completeness limit of our z-band.

The number counts of pBzK and sBzK galaxies are in good agreement with Kong et al. (2006). We find the number of sBzK galaxies increasing steeply with decreasing magnitude, with the slope for the 7C 1756+6520 field similar to K06. 7C 1751+6809, however, shows a small excess (2σ) of sBzK galaxies at bright Ks magnitudes ($19.5 < K\mathrm{s} < 20.5$). The slope of the number counts for pBzK galaxies is similar for both of our radio galaxy fields and Kong et al. (2006). A small excess of Ks-bright pBzK galaxies is suggested in both fields (1.5σ). Such excesses of Ks-bright galaxies have also been noticed around other HzRGs (Kodama et al. 2007). If these Ks-bright sources were associated with the HzRGs, they would be very massive ($M > 10^{11}\ M_{\odot}$) and would represent the massive, evolved galaxy population of a young galaxy cluster around the HzRG. However, the number of sources considered here is too small to reach any firm conclusion since we detect only five pBzK galaxies with $19.5 < K\mathrm{s} < 20.5$. Previous work (K06; Lane et al. 2007; Hartley et al. 2008) has shown that the pBzK number counts show a turn over at $K > 21$ with the counts slope flattening at fainter sources. We also strongly suspect this flattening in our counts although our BzK selection rapidly becomes incomplete at $K\mathrm{s} \geq 21$. A possible explanation for this turn-over is that pBzK galaxies are selected in a small redshift range and consist of very massive, passively evolving galaxies. Due to downsizing, their number decrease at lower luminosities (Hartley et al. 2008). The slope of the counts and the range of Ks magnitudes sampled by the pBzK* galaxies are also consistent with the pBzK galaxies, suggesting that our extended selection criteria is also likely to be selecting galaxies in the same redshift range.

4. Properties of candidate massive cluster members

4.1. Spatial distribution

Figure 8 displays the spatial distribution of the candidates around the radio galaxies. We also plot all the sources detected (3σ) in B, z and Ks (black dots) in order to visualize the zones of the field affected by our cross-talk flag (see Fig. 2) and very

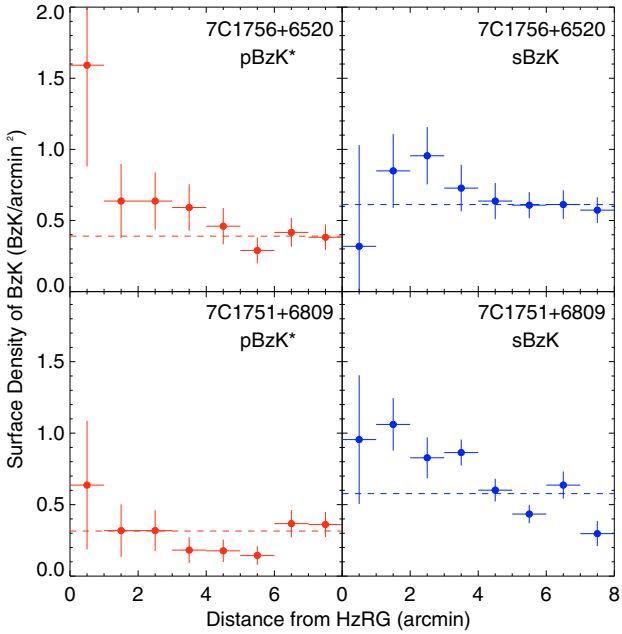

Fig. 9. Radial density profile of BzK selected galaxies around 7C1756+6520 (*upper panels*) and 7C 1751+6809 (*lower panels*) for pBzK* galaxies (*left panels*) and sBzK galaxies (*right panels*). The full field density is shown by the horizontal dashed lines. The profiles and surface densities were derived from the entire sample of candidates. The values obtained are therefore higher than in Table 1 where the study was restricted to the completeness limit. The error bars indicate the 1σ errors on the counts assuming Poissonian errors.

bright stars. In both fields, the BzK source distribution is clearly inhomogenous. In the 7C 1756+6520 field, the passive candidates (Fig. 8; top left panel) are more numerous in the surroundings of the radio galaxy than in the rest of the field. This was also seen in Sect. 3.3 and Table 2. Eight pBzK* galaxies are roughly aligned with the HzRG in a small E/W structure ~2.5′ in length. Two other excesses are also observed in the field, one ~3′ SE of the HzRG and another one at ~6.5′ NW of the HzRG. These excesses appear to be aligned with a global overdensity of pBzK* galaxies along a large structure in a NW-SE direction. In contrast, no clear excess of pBzK* galaxies is detected in the 7C 1751+6809 field (Fig. 8; bottom left panel) even though they show a relatively non-uniform distribution. We note that one pBzK* galaxy is found near the line of sight to both HzRGs (at 2.4″ for 7C 1756+6520 and 6.3″ for 7C 1751+6809), suggesting that both HzRGs may have close companions.

The sBzK galaxies also have an inhomogenous distribution though it is less well defined than the pBzK* galaxies. In particular, 7C 1756+6520 has nine sBzK galaxies along the same elongated structure near the HzRG. One sBzK galaxy is also found near the line of sight of the HzRG (at ~5.5″, Fig. 12). The sBzK galaxies in the 7C 1751+6809 field show an excess near the center of the field with an elongation in the direction NW-SE with no obvious correlation with the pBzK* spatial distribution. This overdensity was not seen with the density counts in Table 2, most probably due to the fact that the HzRG is at the "edge" of the elongated structure of sBzK galaxies. If associated with the HzRG, this structure would have a ~4 Mpc extent.

Figure 9 presents the radial distribution of pBzK* and sBzK galaxies around both HzRGs i.e., the number of candidates found per radius bin (binsize = 1′) divided by the corresponding ring area. The large error bars are due to the small number

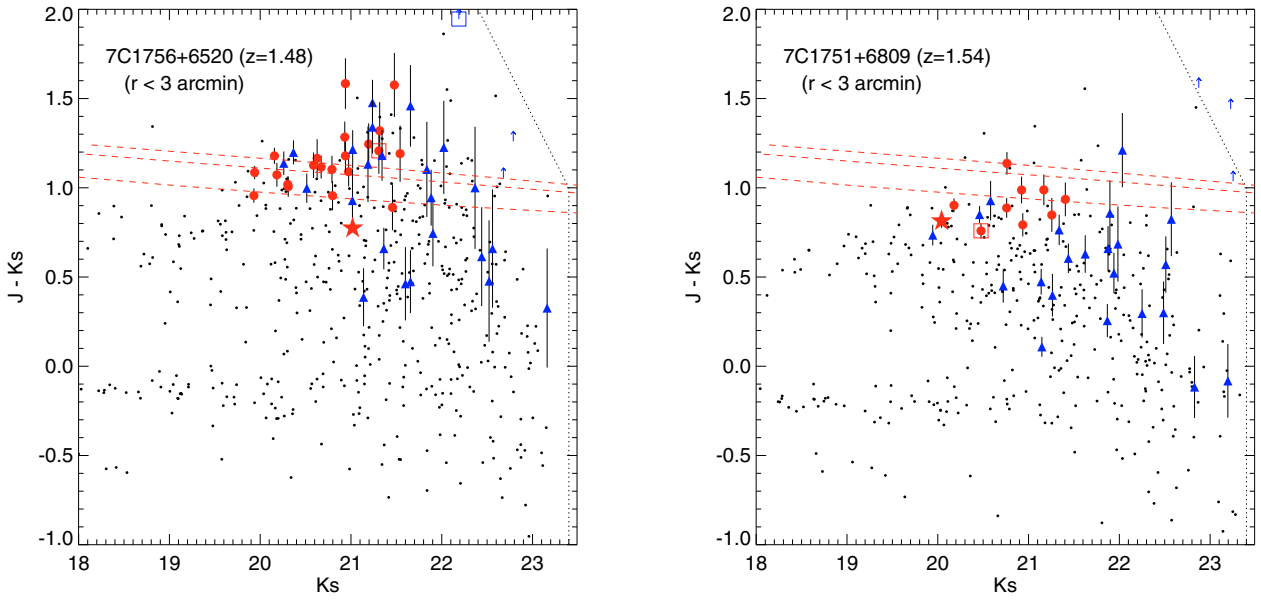

Fig. 10. Color−magnitude diagram ($J - Ks$ vs. Ks) of the regions surrounding the HzRGs (within 3′). The pBzK* and sBzK galaxies are plotted as red circles and blue triangles respectively. sBzK galaxies not detected in J are shown as blue arrows. Also plotted are all sources in this same region detected in the three BzK bands (black dots). The radio galaxies are shown as red stars. The dotted lines represent the 3σ detection limits in J and Ks reported in Sect. 2.2.3. The two pBzK galaxies found near the line of sight of both HzRGs and the sBzK galaxy found near 7C 1756+6520 are indicated by the red and blue squares, respectively. The dashed lines indicate the expected locations of the red sequence at $z = 1.5$ corresponding to the predicted color of a passively evolving stellar population with $z_f = 3, 4$ and 5 (*from lower to upper curve*; see text for details).

of sources used to derive the radial profiles, e.g., only 5 pBzK* and 1 sBzK galaxies are found within 1′ of 7C 1756+6520. The distribution of candidates near 7C 1756+6520 forms an elongated structure, not centered around the HzRG. The radial profile in Fig. 9 is therefore a lower limit to the true concentration of BzK around the HzRG as it does not fully reflect the complex spatial distribution of the sources. However, we note that a clear peak of pBzK* galaxies is seen near the HzRG. The pBzK* density decreases with radius and asymptotes to the full field density (red dashed line) at ∼5′ from the radio galaxy. Variations are also observed in the profile of the sBzK galaxies with a deficit of sources near the HzRG (<1′) and a "bump" in the profile between 2′ and 4′, suggestive of some segregation in the properties of the galaxies in the large scale structure. We note however that the significance of those variations is less that 1σ. As seen previously, no significant variation of the pBzK* density is seen around 7C 1751+6809 but a small overdensity of sBzK is observed within 5′ of the HzRG (1σ significant though).

4.2. Color–magnitude diagram

Color–magnitude diagrams (CMDs) are an efficient method to study the formation and evolution of galaxies. At $z < 1$, galaxy cluster cores are dominated by massive, passively-evolving elliptical galaxies that trace a clear red sequence on the color−magnitude diagram. In the last decade, studies have shown that this red sequence of early-type galaxies is also found in galaxy clusters out to $z \sim 1.5$ (e.g. Mei et al. 2006; Stanford et al. 2006; Tanaka et al. 2007; Lidman et al. 2008). Recent work at even higher redshifts have studied the evolved galaxy population in $z \sim 2$ galaxy clusters and conclude that the red sequence may appear between $z = 3$ and 2 (Kodama et al. 2007; Zirm et al. 2008). We have investigated the CMD of the sources in the region surrounding the HzRGs. Their CMDs are shown in Fig. 10. Sources within 3′ of the HzRGs and with a 3σ detection in all BzK bands are plotted as black dots. The size of the studied region was chosen as a compromise between selecting sources close to the HzRG and including the majority of the candidates in the apparent central overdensity. We note that the region of the CMD at faint Ks magnitude starts to be empty well before the magnitude limit of our Ks-band data due to the non detection of faint Ks sources in the optical bands. pBzK* and sBzK galaxies within 3′ (∼1.5 Mpc at $z = 1.5$) are plotted as red points and blue triangles, respectively. All pBzK* galaxies found near the HzRGs have a $>3\sigma$ detection in the J-band; sBzK galaxies with lower limits in J are marked as blue arrows. The two pBzK* galaxies found near both HzRGs and the sBzK galaxy found near 7C 1756+6520 are marked as squares. We overplot models of the expected location of the red sequence at $z = 1.5$, i.e., the predicted $J - K$ color of a passively evolving galaxy with different formation redshifts ($z_f = 3, 4, 5$; provided by Kodama). The models reproduce the red sequence of passively evolving galaxies in the Coma cluster at $z = 0$ and include a metallicity-magnitude dependance which causes the red sequence slope (Kodama et al. 1998).

The pBzK* galaxies in the inner 3′ region around 7C 1756+6520 have colors consistent with passively evolving galaxies with $z_f \geq 2$ in contrast to the pBzK* galaxies around 7C 1751+6809 which have bluer $J - Ks$ colors. Some elliptical candidates have slightly redder colors ($J - Ks > 1.2$) and may be background objects since the BzK criteria is designed to select objects at $1.4 < z < 2.5$. Two of the pBzK* and three of the sBzK galaxies have $(J - K)_{\rm Vega} > 2.3$ and would be classified as DRGs, i.e., they are likely to be either passive elliptical or dusty star-forming galaxies at $z > 2$.

Recent observations of some high redshift galaxy clusters have shown a deficit of red galaxies at the faint end of the red sequence compared to local clusters (Kajisawa et al. 2000;

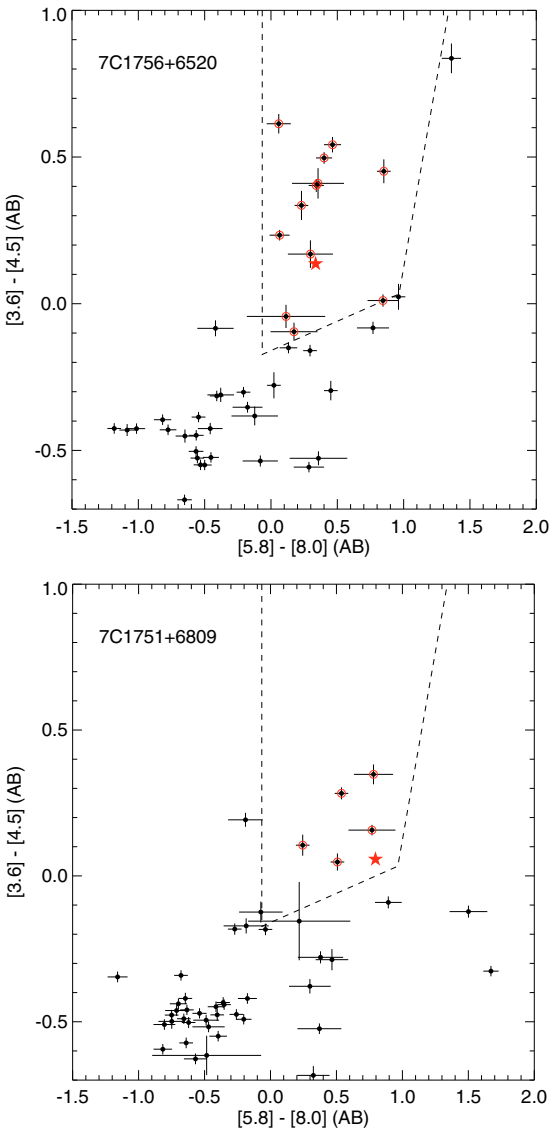

Fig. 11. Mid-IR color−color diagram for 7C 1756+6520 (*top*) and 7C 1751+6809 (*bottom*). All sources with a 5σ detection in all four IRAC bands are plotted. We overplot the Stern et al. (2005) wedge for AGN selection. Sources circled in red are identified as AGN candidates by this criterion. HzRGs are indicated by the red stars and are both found in the selection wedge, as expected.

De Lucia et al. 2007; Tanaka et al. 2005, 2007). It has been suggested that the red sequence appears at bright magnitudes and progressively extends to fainter magnitudes with time. Tanaka et al. (2007) studied a possible large-scale structure around a galaxy cluster at $z = 1.24$ and found that a deficit of faint red galaxies is noted in the clumps surrounding the central cluster but not in the CMD of the cluster itself, suggesting that the build-up of the red sequence is dependent on environment, progressing more rapidly in higher density environments. Considering the potential cluster around 7C 1756+6520, we note a clear deficit of Ks-faint pBzK* galaxies. No pBzK* galaxy is found with $Ks > 21.5$ near the HzRG. At these faint Ks magnitudes, we surely reach the combined incompleteness of our z and Ks bands data. But, as described in Sect. 3.2, we are more than 60% complete at our magnitude limits. For example, 29 pBzK* galaxies with $Ks > 21.5$ are found in the full field and sBzK galaxies are found with $Ks > 21.5$ within 3′ of the HzRG. We therefore conclude that the truncation at faint magnitudes is real. This would imply that this is another example of downsizing (Cowie et al. 1996); i.e., the more massive cluster members stopped their star-formation earlier than the less massive cluster members. A similar study of the CMD of red galaxies in the field of the X-ray galaxy cluster XMMUJ2235.3-2557 at $z = 1.39$ is presented in Lidman et al. (2008). They do not observe evidence of a truncation of the red sequence at fainter magnitudes, suggesting that they are looking at a richer or more evolved system. The scatter of the pBzK* galaxies relative to the red sequence model at $z_f = 5$ ($z_f = 4$) is 0.089 ± 0.067 (0.095 ± 0.061) magnitudes for non-DRG galaxies. This scatter is large and most probably inflated by non-cluster members. Studies of the intrinsic scatter of the red sequence in galaxy clusters at $1.2 < z < 1.5$ have however shown that the scatter in $J - K$ can be up to ∼0.06 (Lidman et al. 2004, 2008).

We stress that the pBzK* galaxies selected in this work are only candidate cluster members and that spectroscopic follow-up will be necessary to confirm their physical association to the HzRGs.

5. AGN candidates

Recent studies suggest that AGN companions are often found around radio galaxies. Croft et al. (2005) spectroscopically confirmed three QSOs in the surroundings of PKS 1138-262 at $z = 2.16$ and suggested that the QSOs were triggered by the protocluster formation (see also Pentericci et al. 2000). Venemans et al. (2007) also detected QSOs near radio-galaxies at $z > 3$. Recently, Galametz et al. (2009a) studied the AGN population in a large sample of galaxy clusters at $z < 1.5$ and found an excess of AGN within 0.5 Mpc of the cluster centers, with the number of AGN in clusters increasing with redshift (see also Eastman et al. 2007). Powerful AGN provide an alternative way to look for relatively massive host galaxies in a complementary technique to the near-IR color selection.

Stern et al. (2005) presents a robust technique for identifying active galaxies from mid-infrared color criteria (see also Lacy et al. 2004). While the continuum emission of stellar populations peaks at approximately 1.6 μm, the continuum of AGN is dominated by a power law throughout the mid-infrared. Stern et al. (2005) adopt the following (Vega system) criteria[7] to isolate AGN from other sources: $([5.8]-[8.0]) > 0.6 \cap ([3.6]-[4.5]) > 0.2 \times ([5.8]-[8.0]) + 0.18 \cap ([3.6]-[4.5]) > 2.5 \times ([5.8]-[8.0]) - 3.5$ Since the criterion is designed to identify power-law spectra, they do not preferentially select AGN in any specific redshift range. We apply this selection criteria to all sources with a 5σ detection in all four IRAC bands. The coordinates of the selected AGN for 7C 1756+6520 (12 candidates) and 7C 1751+6809 (5 candidates) are given in Table 3 and Table 4, respectively. Figure 11 shows their distributions in the [3.6]−[4.5] vs [5.8]−[8.0] color−color diagram. We note that although neither HzRG is detected at a 5σ level in the 5.8 μm-band, their IRAC magnitudes and position in the IRAC color−color diagram are presented in the tables and in Fig. 11. Both are undeniably classified as AGN by the Stern et al. (2005) criterion.

As a comparison field, we use the IRAC Shallow Survey (ISS; Eisenhardt et al. 2004), which includes four IRAC bands and covers 8 square degrees in the Boötes field with at least

[7] We use the following conversions between the Vega and AB photometric systems: $[3.6]_{AB} = [3.6]_{Vega} + 2.792$, $[4.5]_{AB} = [4.5]_{Vega} + 3.265$, $[5.8]_{AB} = [5.8]_{Vega} + 3.733$ and $[8.0]_{AB} = [8.0]_{Vega} + 4.399$.

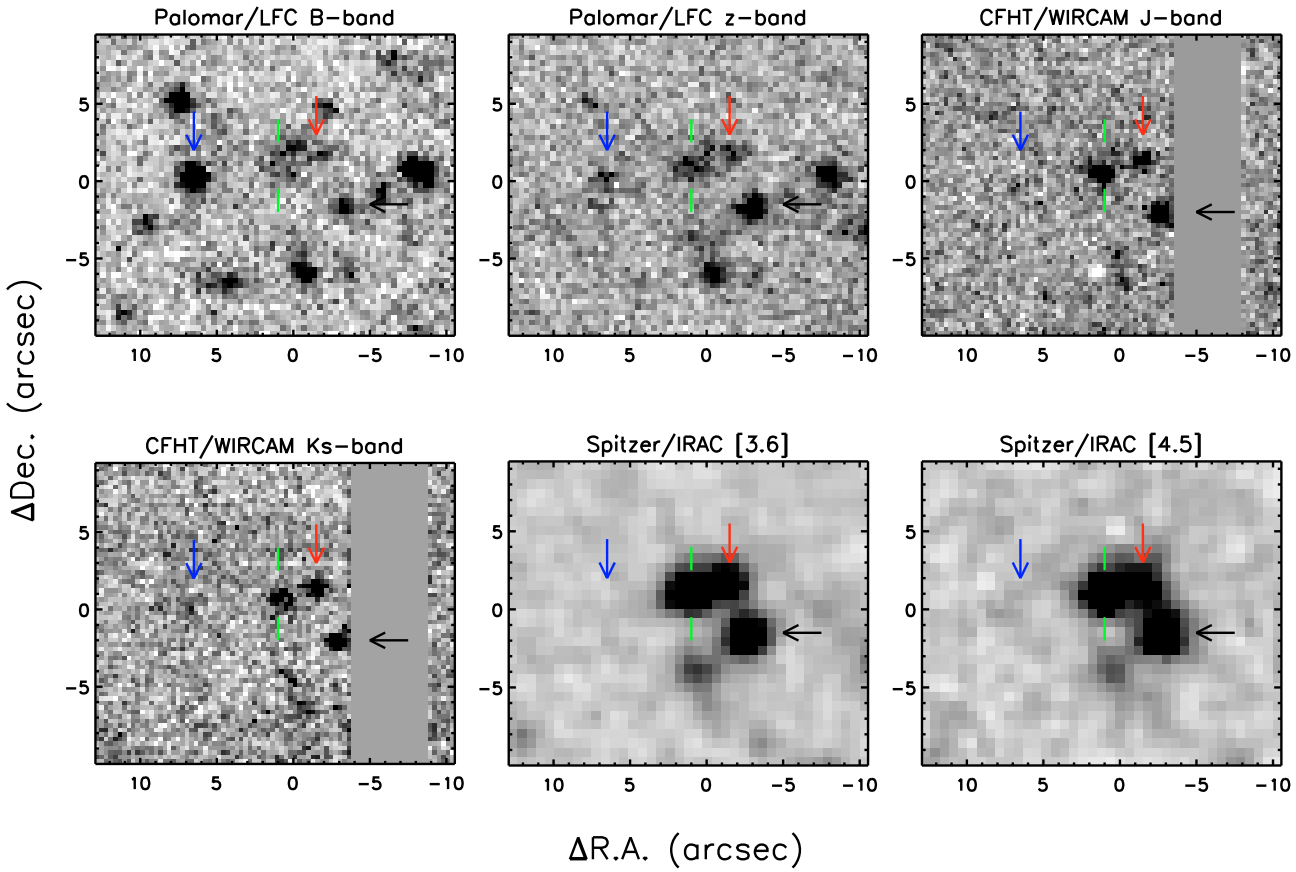

Fig. 12. 7C 1756+6520 and its immediate surroundings in our Palomar/LFC *B* and *z*-bands, CFHT/WIRCAM *J* and *K*s-bands, and Spitzer/IRAC 3.6 μm and 4.5 μm images. *North is up and East is to the left*. 7C 1756+6520 is indicated by the green marks. The s*BzK* galaxy, p*BzK* galaxy and AGN candidate found near the HzRG are marked by the blue, red and black arrows, respectively.

90 s exposure time per position. 2262 sources in ISS are found in the Stern et al. (2005) AGN selection wedge, where we require a 5σ detections in all four IRAC bands (Galametz et al. 2009a). The 5.8 μm band is the least sensitive with a 5σ limiting depth of 15.9 (Vega, in an aperture-corrected 3″ diameter aperture; equivalent to 51 μJy). Whereas we would expect three to four AGN candidates in the HzRG fields, we find 8 AGN candidates near 7C 1756+6520 and four near 7C 1751+6809 at the depth of ISS. We therefore observe an overdensity of AGN candidates in the field of 7C 1756+6520 by a factor of two compared to the 7C 1751+6809 and ISS fields. One AGN candidate is found only 5″ offset from 7C 1756+6520 (Fig. 12, Sect. 6) and two additional candidates are found within 1.5′ of the HzRG. However, the 12 AGN candidates do not show any particular spatial distribution as was seen for both the p*BzK** and s*BzK* galaxies (see Sect. 4.2). No AGN candidate is found within 1.5′ of 7C 1751+6809.

6. Candidate close companions to 7C 1756+6520

An elliptical, a star-forming and an AGN candidate are found near the line of sight to 7C 1756+6520 (within 6″), suggestive of several close companions. Figure 12 shows the immediate surroundings of 7C 1756+6520 in our imaging bands; arrows indicate the p*BzK** galaxies, s*BzK* galaxies and the AGN candidate. Using the density of *BzK* galaxies found in the full field, we find that the probability of finding a p*BzK** galaxy within 6″ of the HzRG is ~0.44%, and the probability of finding a s*BzK* galaxy is ~0.54%. At the depth of our IRAC data, the probability of finding an AGN candidate in the same area is ~0.57%. The probability of finding the three candidates in this small area around the HzRG is therefore extremely small, strongly suggesting that these candidates are associated with the HzRG and form a very unique and diverse system of bound galaxies.

7. Conclusions

We study of the surroundings of two radio galaxies at $z \sim 1.5$ using deep multiwavelength imaging. We select candidate cluster members using color selection techniques designed to select galaxies at the redshift of the targeted HzRG. This technique has been proven to identify clusters and proto-clusters at high redshift ($z > 2$; Kajisawa et al. 2006; Tanaka et al. 2007). An excess of candidate passive elliptical candidates is found in the field of one of our two targets, 7C 1756+6520 by a factor of 3.1 ± 0.8 compared to control fields. A study of the counts-in-cells fluctuations in our larger control field shows that the probability to find such an overdensity in the field is very low (0.26%). These results may be compared to previous studies that have been made at similar or higher redshifts. The Best et al. (2003) study of the environments of six radio-loud AGN at $z \sim 1.6$ finds an excess by a factor of 1.5 to 4 of EROs within radial distances of ~1 Mpc of the AGN. Similarly, Kodama et al. (2007) select passive evolving and star forming cluster member candidates in the surroundings of four HzRGs with $2 < z < 3$ applying color cuts in *JHK*s and found excesses by a factor of two to three compared to the field. Clusters were already suspected around those HzRGs in previous studies that were concentrated on

overdensities of narrow-band (Hα, Lyα) emitters also by a factor of two to five larger than in the field (Kurk et al. 2004a; Venemans et al. 2005, 2007). Looking at narrow-band emitters has been very efficient at finding overdensities around HzRGs. However, such clusters members, dominated by young stellar populations, are likely not the most massive members of the galaxy clusters. Indeed, recent studies show that Lyα emitters have rather small stellar masses. Finkelstein et al. (2007) found masses ranging from 2×10^7 to 2×10^9 $M_\odot$ for a sample of 98 Lyα emitters at $z \sim 4.5$. Similar masses were deduced from Lyα emitters in Gawiser et al. (2007) who found stellar masses of 10^9 $M_\odot$ for lower redshift objects ($z \sim 3.1$). Looking at the properties of Lyα emitters, members of a protocluster at $z = 4.1$, Overzier et al. (2008) derived a mean stellar mass of $\sim 10^{8-9}$ $M_\odot$ based on stacked Ks-band images, indicating that Lyα emitters in the field and in protoclusters at high redshift have similar masses. Kurk et al. (2004b) used near infrared magnitudes to derive the stellar masses of Hα emitters found in the overdensity surrounding PKS 1138-262, a well known protocluster at $z = 2.16$, and found that Hα emitters are more massive than Lyα emitters, with a stellar mass $\sim 2 \times 10^{10}$ $M_\odot$. The total stellar mass derived from both Lyα and Hα emitters around PKS 1138-262 (40 sources) is $\sim 10^{12}$ $M_\odot$ (Kurk et al. 2004b). The mass function of galaxy clusters is in fact dominated by the evolved galaxy population, known to be rarer but much more massive than the narrow-band emitters (e.g., for Ks < 21.5, $M_{\rm stars} > 10^{11}$ $M_\odot$; Kodama et al. 2007). If at $z \sim 1.5$, the two objects with Ks = 20 found within 3′ o2f 7C 1756+6520 would each have a stellar mass of 5×10^{11} $M_\odot$ and would therefore already have a mass equivalent to all the narrow-band emitters found near PKS 1138-262. It is therefore essential to search for this population of red elliptical galaxies to fully understand the earliest phases of cluster formation.

Our study makes use of wide-field optical and near-infrared cameras and permits the investigation of the spatial distribution of potential cluster members over a large area around the HzRG. Indeed, the small field of view of the previous generation of near-infrared instruments limited the study of large-scale structures, clusters and proto-clusters. Recently, Tanaka et al. (2007) presented a study of a large-scale structure around a galaxy cluster at $z = 1.24$ with a possible large (20 Mpc) filamentary structure formed by the main cluster and four possible associated clumps of red galaxies, illustrating the necessity to look at galaxy clusters on larger scales than the cluster itself. The 7C 1756+6520 field presents several overdensities of red objects separated by several arcmin, as well as one nearby the HzRG. However, spectroscopic confirmation of these extended structures being associated and at high redshift is challenging due of the required large field of view on a multi-object spectrograph, and the high redshift which places the main spectral features (emission lines for star-forming and breaks for elliptical galaxies) out of the optical bands. This will hopefully be achieved with the new generation of multi-object, near-infrared spectrographs (e.g., MOIRCS on Subaru).

Acknowledgements. We are very grateful to S. Adam Stanford for useful discussions and Tadayuki Kodama for having provided the models of red sequences presented in this paper. We thank Brigitte Rocca-Volmerange for her support of this project. We would also like to thank Andrea Grazian (and the GOODS-MUSIC team) and Ryan Quadri (and the MUSYC survey team) for useful emails exchanges on their online catalogs. This work is based in part on data products produced at the TERAPIX data center located at the Institut d'Astrophysique de Paris and generated from observations obtained at the Canada-France-Hawaii Telescope (CFHT) which is operated by the National Research Council of Canada, the Institut National des Sciences de l'Univers of the Centre National de la Recherche Scientifique of France, and the University of Hawaii. It is also based on observations obtained at the Hale 200 inch telescope at Palomar Observatory and on observations made with the *Spitzer Space Telescope*, which is operated by the Jet Propulsion Laboratory, California Institute of Technology under a contract with NASA.

References

Abraham, R. G., Glazebrook, K., McCarthy, P. J., et al. 2004, AJ, 127, 2455
Bertin, E., & Arnouts, S. 1996, A&AS, 117, 393
Best, P. N., Lehnert, M. D., Miley, G. K., & Röttgering, H. J. A. 2003, MNRAS, 343, 1
Borgani, S., Rosati, P., Tozzi, P., et al. 2001, ApJ, 561, 13
Bruzual, G., & Charlot, S. 2003, MNRAS, 344, 1000
Cardelli, J. A., Clayton, G. C., & Mathis, J. S. 1989, ApJ, 345, 245
Carilli, C. L., Harris, D. E., Pentericci, L., et al. 2002, ApJ, 567, 781
Cimatti, A., Daddi, E., Mignoli, M., et al. 2002, A&A, 381, L68
Cimatti, A., Auvergne, M., Baglin, A., et al. 2008, A&A, 482, 21
Cool, R. J. 2007, ApJS, 169, 21
Cowie, L. L., Songaila, A., Hu, E. M., & Cohen, J. G. 1996, AJ, 112, 839
Croft, S., Kurk, J., van Breugel, W., et al. 2005, AJ, 130, 867
Daddi, E., Cimatti, A., Pozzetti, L., et al. 2000, A&A, 361, 535
Daddi, E., Cimatti, A., Renzini, A., et al. 2004, ApJ, 617, 746
De Lucia, G., Poggianti, B. M., Aragón-Salamanca, A., et al. 2007, MNRAS, 374, 809
Eastman, J., Martini, P., Sivakoff, G., et al. 2007, ApJ, 664, L9
Eisenhardt, P. R., Stern, D., Brodwin, M., et al. 2004, ApJS, 154, 48
Eke, V. R., Cole, S., Frenk, C. S., & Patrick Henry, J. 1998, MNRAS, 298, 1145
Elston, R. J., Gonzalez, A. H., McKenzie, E., et al. 2006, ApJ, 639, 816
Fazio, G. G., Hora, J. L., Allen, L. E., et al. 2004, ApJS, 154, 10
Finkelstein, S. L., Rhoads, J. E., Malhotra, S., Pirzkal, N., & Wang, J. 2007, ApJ, 660, 1023
Finlator, K., Ivezić, Ždeljko; F. X., et al. 2000, AJ, 120, 2615
Fioc, M., & Rocca-Volmerange, B. 1997, A&A, 326, 950
Franx, M., Labbé, I., Rudnick, G., et al. 2003, ApJ, 587, L79
Galametz, A., Stern, D., Eisenhardt, P. R. M., et al. 2009a, ApJ, 694, 1309
Gawiser, E., van Dokkum, P. G., Herrera, D., et al. 2006, ApJS, 162, 1
Gawiser, E., Francke, H., Lai, K., et al. 2007, ApJ, 671, 278
Gehrels, N. 1986, ApJ, 303, 336
Grazian, A., Fontana, A., Moscardini, L., et al. 2006a, A&A, 453, 507
Grazian, A., Fontana, A., de Santis, C., et al. 2006b, A&A, 449, 951
Grazian, A., Salimbeni, S., Pentericci, L., et al. 2007, A&A, 465, 393
Hartley, W. G., Lane, K. P., Almaini, O., et al. 2008, MNRAS, 391, 1301
Imai, K., Pearson, C. P., Matsuhara, H., et al. 2008, ApJ, 683, 45
Kajisawa, M., Yamada, T., Tanaka, I., et al. 2000, PASJ, 52, 61
Kajisawa, M., Kodama, T., Tanaka, I., Yamada, T., & Bower, R. 2006, MNRAS, 371, 577
Kodama, T., Arimoto, N., Barger, A. J., & Arag'on-Salamanca, A. 1998, A&A, 334, 99
Kodama, T., Tanaka, I., Kajisawa, M., et al. 2007, MNRAS, 377, 1717
Kong, X., Daddi, E., Arimoto, N., et al. 2006, ApJ, 638, 72
Kurk, J. D., Pentericci, L., Overzier, R. A., Röttgering, H. J. A., & Miley, G. K. 2004a, A&A, 428, 817
Kurk, J. D., Pentericci, L., Röttgering, H. J. A., & Miley, G. K. 2004b, A&A, 428, 793
Kurk, J. D., Cimatti, A., Daddi, E., et al. 2008, in Infrared Diagnostics of Galaxy Evolution, ASP Conf. Ser., 381, 303
Lacy, M., Rawlings, S., & Warner, P. J. 1992, MNRAS, 256, 404
Lacy, M., Rawlings, S., Hill, G. J., et al. 1999, MNRAS, 308, 1096
Lacy, M., Storrie-Lombardi, L. J., Sajina, A., et al. 2004, ApJS, 154, 166
Lacy, M., Wilson, G., Masci, F., et al. 2005, ApJS, 161, 41
Landolt, A. U. 1992, AJ, 104, 340
Lane, K. P., Almaini, O., Foucaud, S., et al. 2007, MNRAS, 379, L25
Lidman, C., Rosati, P., Demarco, R., et al. 2004, A&A, 416, 829
Lidman, C., Rosati, P., Tanaka, M., et al. 2008, A&A, 489, 981
Maihara, T., Iwamuro, F., Tanabe, H., et al. 2001, PASJ, 53, 25
Makovoz, D., & Khan, I. 2005, in Astronomical Data Analysis Software and Systems XIV, ed. P. Shopbell, M. Britton, & R. Ebert, ASP Conf. Ser., 347, 81
Marmo, C. 2007, in Astronomical Data Analysis Software and Systems XVI, ed. R. A. Shaw, F. Hill, & D. J. Bell, ASP Conf. Ser., 376, 285
Matthews, T. A., Morgan, W. W., & Schmidt, M. 1964, ApJ, 140, 35
Mei, S., Holden, B. P.,; Blakeslee, J. P., et al. 2006, ApJ, 644, 759
Metcalfe, N., Shanks, T., Fong, R., & Jones, L. R. 1991, MNRAS, 249, 498
Metcalfe, N., Shanks, T., Fong, R., & Roche, N. 1995, MNRAS, 273, 257
Miley, G. K., Overzier, R. A., Tsvetanov, Z. I., et al. 2004, Nature, 427, 47
Mobasher, B., Idzi, R., Benítez, N., et al. 2004, ApJ, 600, L167
Monet, D. G., Levine, S. E., Canzian, B., et al. 2003, AJ, 125, 984
Mullis, C. R., Rosati, P., Lamer, G., et al. 2005, ApJ, 623, L85
Overzier, R. A., Bouwens, R. J., Cross, N. J. G., et al. 2008, ApJ, 673, 143
Pentericci, L., Kurk, J. D., Röttgering, H. J. A., et al. 2000, A&A, 361, L25

Puget, P., et al. 2004, in Ground-based Instrumentation for Astronomy, ed. A. F. M. Moorwood, & I. Masanori, Proc. SPIE, 5492, 978
Quadri, R., Marchesini, D., van Dokkum, P., et al. 2007, AJ, 134, 1103
Reddy, N. A., Steidel, C. C., Fadda, D., et al. 2006, ApJ, 644, 792
Rettura, A., et al. 2008, ApJ, 806
Santini, P., et al. 2009, ArXiv e-prints
Schlegel, D. J., Finkbeiner, D. P., & Davis, M. 1998, ApJ, 500, 525
Seymour, N., Stern, D., De Breuck, C., et al. 2007, ApJS, 171, 353
Simcoe, R. A., Metzger, M. R., Small, T. A., & Araya, G. 2000, in BAAS, 32, 758
Skrutskie, M. F., et al. 1997, in The Impact of Large Scale Near-IR Sky Surveys, ed. F. Garzon, N. Epchtein, A. Omont, B. Burton, & P. Persi, Ap&SS Library, 210, 25
Stanford, S. A., Romer, A. K., Sabirli, K., et al. 2006, ApJ, 646, L13
Stern, D., Holden, B., Stanford, S. A., & Spinrad, H. 2003, AJ, 125, 2759
Stern, D., Eisenhardt, P., Gorjian, V., et al. 2005, ApJ, 631, 163
Stern, D., Jimenez, R., Verde, L., Kamionkowski, M., & Stanford, S. A. 2009 [arXiv:0907.3149]
Tanaka, M., Kodama, T., Arimoto, N., et al. 2005, MNRAS, 362, 268
Tanaka, M., Kodama, T., Kajisawa, M., et al. 2007, MNRAS, 377, 1206
Teplitz, H. I., McLean, I. S., & Malkan, M. A. 1999, ApJ, 520, 469
Venemans, B. P., Röttgering, H. J. A., Miley, G. K., et al. 2005, A&A, 431, 793
Venemans, B. P., Röttgering, H. J. A., Miley, G. K., et al. 2007, A&A, 461, 823
Williams, R. E., Blacker, B., Dickinson, M., et al. 1996, AJ, 112, 1335
York, D. G., Adelman, J., Anderson, J. E., Jr., et al. 2000, AJ, 120, 1579
Zirm, A. W., Stanford, S. A., Postman, M., et al. 2008, ApJ, 680, 224

Table 2. Surface densities of *BzK* galaxies (to the completeness limits; degrees^{-2}).

Field	GOODS	MUSYC				All	7C 1756+6520		7C 1751+6809	
	MUSIC	ECDFS	EHDFS	SDSS1030	CW1255	MUSYC	Full	$r < 2$ Mpc	Full	$r < 2$ Mpc
Area[a]	143.2	969.6	201.1	106.7	101.9	1379.3	333.4	47.9	336.2	47.7
(1)	(2)	(3)	(4)	(5)	(6)	(7)	(8)	(9)	(10)	(11)
p*BzK*	130 ± 60	70 ± 20	70 ± 40	170 ± 80	35 ± 35	70 ± 10	190 ± 45	330 ± 160	140 ± 40	no detection
p*BzK**	430 ± 100	370 ± 40	320 ± 80	640 ± 150	210 ± 90	370 ± 30	620 ± 80	1160 ± 295	510 ± 70	250 ± 140
s*BzK*	500 ± 110	505 ± 40	480 ± 90	300 ± 100	490 ± 130	485 ± 40	490 ± 70	990 ± 270	350 ± 60	500 ± 190

[a] Area are given in square arcmin.

Table 3. AGN candidates in 7C 1756+6520 field.

ID	RA	Dec.	[3.6]	[4.5]	[5.8]	[8.0]
HzRG	17:57:05.599	+65:19:53.86	20.01	19.87	20.08	19.74
1	17:57:13.152	+65:17:06.43	19.41	19.51	19.64	19.46
2	17:56:52.525	+65:16:56.67	20.12	19.67	19.78	18.93
3	17:56:59.055	+65:17:54.96	19.82	19.48	19.43	19.20
4	17:57:13.186	+65:19:08.40	19.77	19.15	18.51	18.45
5	17:57:33.291	+65:20:25.55	18.77	18.76	18.95	18.10
6	17:56:55.862	+65:19:06.56	18.32	17.82	17.56	17.16
7	17:57:30.881	+65:21:21.77	18.98	18.57	17.98	17.64
8	17:57:30.462	+65:21:21.75	19.12	18.58	17.97	17.50
9	17:57:04.981	+65:19:51.00	20.02	19.61	19.69	19.34
10	17:57:20.156	+65:21:56.79	20.16	19.99	19.63	19.33
11	17:57:15.439	+65:21:56.02	19.13	19.17	19.73	19.62
12	17:56:41.147	+65:22:59.14	17.48	17.24	18.42	18.36

Table 4. AGN candidates in 7C 1751+6809 field.

ID	RA	Dec.	[3.6]	[4.5]	[5.8]	[8.0]
HzRG	17:50:50.024	+68:08:26.47	19.68	19.63	20.78	19.99
1	17:50:51.439	+68:06:06.59	18.52	18.23	18.56	18.02
2	17:51:24.879	+68:08:34.08	19.99	19.88	19.72	19.47
3	17:50:39.182	+68:06:47.57	19.41	19.36	19.23	18.72
4	17:50:34.238	+68:10:23.56	19.50	19.15	19.14	18.36
5	17:50:51.762	+68:10:57.72	17.40	17.24	19.59	18.82

Table 5. pBzK* galaxies in 7C 1756+6520 field.

ID	RA	Dec.	B	z	J	Ks
1	17:57:46.32	65:13:54.5	26.69[a]	21.55	20.60	20.11
2	17:58:01.68	65:15:14.7	26.78	22.39	20.93	20.15
3	17:55:50.88	65:16:20.6	24.63	22.91	21.16	20.33
4	17:58:10.56	65:16:56.6	25.65	22.71	21.59	20.57
5	17:57:19.19	65:19:31.1	25.94	22.72	21.57	20.67
6	17:58:26.40	65:19:35.4	26.45	24.22	22.78	21.77
7	17:57:12.48	65:19:45.1	26.65	22.63	21.37	20.18
8	17:56:30.72	65:20:52.4	25.20	23.24	22.43	20.99
9	17:56:16.80	65:21:10.4	23.49	21.90	21.58	20.55
10	17:56:48.48	65:21:22.0	25.01	23.14	22.04	20.97
11	17:56:52.56	65:22:59.5	26.88	23.70	22.55	20.71
12	17:57:01.68	65:16:50.2	>27.1	24.18	22.91	22.03
13	17:57:12.48	65:19:41.9	>27.1	23.04	21.84	20.63
14	17:57:20.40	65:11:51.0	>27.1	23.03	22.08	20.92
15	17:57:12.48	65:12:10.5	>27.1	23.68	22.63	21.30
16	17:57:53.76	65:12:45.7	>27.1	23.29	21.95	21.09
17	17:57:33.12	65:13:13.4	>27.1	24.11	22.58	21.81
18	17:57:28.80	65:13:28.2	>27.1	23.45	21.99	21.18
19	17:57:11.04	65:13:46.9	>27.1	22.25	21.12	20.44
20	17:57:40.08	65:14:08.9	>27.1	23.28	22.30	21.33
21	17:57:41.76	65:14:17.9	>27.1	24.25	22.97	21.71
22	17:57:26.40	65:14:59.3	>27.1	23.88	22.45	21.74
23	17:57:52.56	65:15:16.9	>27.1	23.76	22.93	21.57
24	17:57:40.32	65:15:23.4	>27.1	23.13	21.53	20.51
25	17:57:16.56	65:15:43.9	>27.1	22.79	21.46	20.49
26	17:58:06.48	65:15:47.2	>27.1	23.13	21.96	20.74
27	17:58:13.92	65:15:51.1	>27.1	22.08	20.95	20.11
28	17:56:55.68	65:16:00.5	>27.1	23.81	22.13	21.20
29	17:56:25.44	65:16:36.1	>27.1	23.37	22.80	21.57
30	17:58:19.68	65:16:50.5	>27.1	23.39	21.94	21.20
31	17:57:44.40	65:17:14.3	>27.1	23.80	23.56	21.62
32	17:57:40.08	65:17:17.5	>27.1	23.32	21.84	21.10
33	17:57:33.84	65:17:20.8	>27.1	23.22	22.70	21.58
34	17:56:43.92	65:17:50.6	>27.1	23.43	22.99	21.69
35	17:58:29.04	65:18:25.2	>27.1	22.34	20.83	20.33
36	17:56:32.64	65:18:32.8	>27.1	23.79	22.25	21.46
37	17:56:48.96	65:18:50.8	>27.1	23.70	22.65	21.32
38	17:56:52.32	65:18:52.2	>27.1	22.55	21.21	20.31
39	17:57:28.32	65:19:24.6	>27.1	21.91	20.82	19.93
40	17:57:13.92	65:19:44.1	>27.1	23.16	21.82	20.79
41	17:57:22.80	65:19:45.5	>27.1	23.17	22.39	21.46
42	17:57:58.08	65:19:44.4	>27.1	23.91	22.33	21.40
43	17:57:05.04	65:19:54.5	>27.1	23.47	22.48	21.31
44	17:56:42.72	65:20:27.2	>27.1	23.11	21.91	20.93
45	17:57:21.36	65:20:52.1	>27.1	22.50	21.38	20.30
46	17:57:52.08	65:21:07.9	>27.1	23.70	22.17	21.48
47	17:56:55.44	65:21:15.5	>27.1	22.97	21.78	20.80
48	17:57:40.08	65:21:26.6	>27.1	24.75	22.31	22.10
49	17:58:16.56	65:21:24.1	>27.1	23.18	21.74	20.92
50	17:56:19.44	65:21:25.9	>27.1	22.05	20.52	19.87
51	17:56:35.28	65:21:32.8	>27.1	23.85	22.83	21.33
52	17:56:50.16	65:21:56.9	>27.1	23.88	22.62	21.54
53	17:56:50.16	65:22:05.9	>27.1	23.16	22.22	20.94
54	17:58:36.96	65:22:09.5	>27.1	23.63	22.46	21.20
55	17:56:12.00	65:22:19.9	>27.1	23.45	21.74	21.25
56	17:56:25.20	65:22:23.9	>27.1	24.13	22.69	21.42
57	17:55:31.68	65:22:36.8	>27.1	21.72	21.03	20.14
58	17:55:55.44	65:23:17.5	>27.1	22.99	22.05	21.32
59	17:57:33.36	65:23:21.8	>27.1	24.34	23.25	21.83
60	17:56:54.48	65:23:35.1	>27.1	22.41	21.25	20.23
61	17:58:07.69	65:23:50.6	>27.1	21.89	20.63	19.79
62	17:57:11.04	65:23:56.8	>27.1	23.40	22.51	21.20
63	17:57:25.20	65:23:58.2	>27.1	23.45	22.86	21.76
64	17:56:49.44	65:24:21.2	>27.1	23.41	22.36	21.13
65	17:57:45.84	65:24:34.6	>27.1	23.62	21.77	21.39

Table 5. continued.

ID	RA	Dec.	B	z	J	Ks
66	17:55:42.72	65:24:56.9	>27.1	22.80	21.30	20.43
67	17:58:14.88	65:25:05.2	>27.1	22.59	21.22	20.32
68	17:57:00.00	65:25:12.4	>27.1	23.54	22.16	21.73
69	17:57:54.72	65:25:25.7	>27.1	24.14	22.42	21.53
70	17:55:33.60	65:25:26.4	>27.1	22.99	21.66	20.56
71	17:55:57.84	65:25:37.6	>27.1	22.63	21.51	20.59
72	17:57:39.12	65:25:40.1	>27.1	23.87	23.07	21.62
73	17:55:57.84	65:25:40.8	>27.1	23.65	22.21	21.36
74	17:57:16.08	65:26:01.7	>27.1	23.72	22.19	21.36
75	17:55:55.44	65:26:12.8	>27.1	23.79	22.19	21.43
76	17:55:39.60	65:26:21.8	>27.1	23.32	21.52	20.83
77	17:57:05.28	65:27:21.6	>27.1	23.99	22.63	21.80
78	17:55:29.76	65:27:33.8	>27.1	22.55	21.14	20.41
79	17:55:46.56	65:27:32.8	>27.1	23.65	22.54	21.64
80	17:57:28.80	65:27:34.2	>27.1	23.20	22.42	20.72
81	17:56:58.80	65:27:39.2	>27.1	23.06	22.19	20.44
82	17:55:59.28	65:27:41.8	>27.1	22.63	22.03	20.78
83	17:57:35.04	65:27:38.9	>27.1	23.74	22.16	21.30
84	17:55:57.12	65:27:48.2	>27.1	22.30	20.81	20.18
85	17:55:57.84	65:27:49.0	>27.1	24.36	22.55	21.85
86	17:56:49.68	65:27:56.2	>27.1	22.60	21.37	20.63
87	17:56:42.48	65:28:17.4	>27.1	24.19	22.86	21.62
88	17:56:47.28	65:28:36.5	>27.1	23.48	22.06	21.32
89	17:57:06.00	65:29:08.5	>27.1	23.90	23.24	21.40
90	17:57:34.32	65:11:39.1	>27.1	22.33	20.73	19.78
91	17:57:10.08	65:12:55.4	>27.1	22.81	21.83	20.89
92	17:57:09.84	65:12:59.4	>27.1	23.63	22.73	21.49
93	17:57:36.48	65:13:50.2	>27.1	23.85	22.20	21.32
94	17:58:14.64	65:13:46.6	>27.1	24.21	22.10	21.00
95	17:56:41.04	65:13:55.9	>27.1	23.91	21.91	20.98
96	17:57:46.56	65:13:56.3	>27.1	22.46	21.05	20.25
97	17:57:34.56	65:14:06.4	>27.1	23.83	22.59	21.18
98	17:56:25.68	65:14:45.6	>27.1	23.93	21.77	21.30
99	17:57:59.28	65:15:07.9	>27.1	23.44	22.46	21.03
100	17:57:19.44	65:15:24.5	>27.1	23.54	22.48	21.45
101	17:57:53.76	65:15:33.1	>27.1	23.45	22.21	21.02
102	17:56:53.04	65:15:38.9	>27.1	24.05	22.25	21.31
103	17:58:14.88	65:15:55.5	>27.1	23.18	21.64	20.29
104	17:57:26.16	65:17:08.5	>27.1	23.07	21.68	20.60
105	17:57:51.36	65:17:17.9	>27.1	22.78	21.52	20.46
106	17:57:21.12	65:17:24.7	>27.1	21.95	21.02	19.94
107	17:57:59.76	65:18:01.8	>27.1	23.70	22.07	21.16
108	17:55:27.12	65:18:25.6	>27.1	23.61	21.80	21.03
109	17:56:33.60	65:18:31.0	>27.1	23.94	22.12	21.18
110	17:58:21.12	65:19:13.8	>27.1	22.86	21.52	20.31
111	17:57:29.28	65:19:33.6	>27.1	22.70	21.30	20.16
112	17:57:10.08	65:20:39.5	>27.1	23.78	22.58	21.48
113	17:56:53.76	65:21:07.5	>27.1	23.76	22.40	21.20
114	17:58:22.80	65:21:31.3	>27.1	22.41	20.66	19.95
115	17:56:55.20	65:21:54.0	>27.1	23.65	21.54	20.59
116	17:56:45.84	65:22:27.5	>27.1	23.42	21.49	20.71
117	17:57:02.40	65:22:40.4	>27.1	23.42	22.80	20.94
118	17:57:12.48	65:23:25.8	>27.1	23.42	21.83	20.58
119	17:56:46.80	65:24:14.8	>27.1	23.29	21.48	20.69
120	17:58:11.04	65:24:22.7	>27.1	23.72	22.77	21.36
121	17:56:18.96	65:24:50.4	>27.1	23.91	22.89	21.34
122	17:57:58.56	65:24:52.9	>27.1	23.55	21.78	20.96
123	17:56:16.56	65:25:41.9	>27.1	23.79	22.87	21.47
124	17:55:55.20	65:26:33.3	>27.1	22.44	21.36	20.48
125	17:56:50.16	65:27:05.0	>27.1	23.71	22.70	21.23
126	17:56:33.36	65:27:03.2	>27.1	22.20	21.04	20.11
127	17:56:15.12	65:27:56.5	>27.1	22.93	21.63	20.52
128	17:56:13.20	65:28:44.8	>27.1	22.70	21.20	20.19
129	17:57:48.72	65:29:17.9	>27.1	22.98	21.43	20.01

[a] Magnitudes are derived using SExtractor MAG_AUTO, with the appropriate Galactic extinction correction applied. The color selection for pBzK* galaxies has been made from aperture magnitudes which give slightly different values.

Table 6. pBzK* galaxies in 7C 1751+6809 field.

ID	RA	Dec.	B	z	J	Ks
1	17:51:44.88	67:59:43.1	25.24[b]	23.73	22.58	21.05
2	17:51:07.92	68:04:10.9	25.82	22.36	21.12	20.16
3	17:49:31.44	68:11:44.5	24.74	22.67	21.59	20.47
4	17:51:31.68	68:11:42.7	25.17	24.10	22.51	21.30
5	17:49:57.37	68:13:54.5	24.40	21.77	20.98	19.81
6	17:50:52.08	68:15:00.7	25.35	22.37	60.86	20.07
7	17:50:05.76	68:16:30.4	24.22	22.96	21.71	20.70
8	17:51:49.92	68:17:51.4	24.54	23.33	21.86	20.53
9	17:50:09.12	67:58:32.2	>27.1	23.93	22.96	21.10
10	17:51:38.65	67:58:41.2	>27.1	24.51	22.31	21.43
11	17:49:57.12	67:59:24.3	>27.1	23.94	22.39	21.33
12	17:51:50.64	68:01:09.8	>27.1	22.62	21.36	20.57
13	17:50:32.16	68:01:21.4	>27.1	24.21	22.35	21.29
14	17:51:06.48	68:01:28.9	>27.1	22.77	21.67	20.85
15	17:51:24.96	68:02:54.2	>27.1	22.22	21.31	20.07
16	17:51:43.20	68:03:38.5	>27.1	22.85	21.61	20.90
17	17:49:00.00	68:04:08.4	>27.1	22.24	21.48	20.51
18	17:51:19.44	68:04:14.9	>27.1	24.07	21.75	21.59
19	17:52:10.56	68:04:24.6	>27.1	24.07	21.95	21.88
20	17:49:42.48	68:04:32.5	>27.1	24.74	22.41	21.83
21	17:52:21.36	68:04:39.0	>27.1	23.67	22.08	20.80
22	17:50:19.44	68:05:04.9	>27.1	24.23	22.71	21.37
23	17:48:53.52	68:05:08.5	>27.1	23.30	22.03	21.28
24	17:49:42.00	68:05:11.1	>27.1	22.93	21.42	20.66
25	17:49:38.16	68:05:25.4	>27.1	23.86	21.96	21.18
26	17:50:35.52	68:06:08.6	>27.1	23.52	22.14	21.17
27	17:51:19.44	68:06:30.6	>27.1	23.66	22.15	21.00
28	17:51:52.80	68:07:06.6	>27.1	21.75	20.94	19.63
29	17:51:04.56	68:07:06.6	>27.1	23.25	21.73	20.76
30	17:49:10.56	68:07:18.1	>27.1	23.16	21.99	20.91
31	17:52:22.56	68:07:51.6	>27.1	24.63	22.13	20.98
32	17:49:01.68	68:07:58.1	>27.1	24.03	22.04	21.35
33	17:50:49.92	68:08:26.2	>27.1	22.40	21.11	20.04
34	17:51:13.93	68:08:27.6	>27.1	22.67	20.83	20.18
35	17:48:52.32	68:08:26.2	>27.1	24.12	22.16	21.11
36	17:51:13.44	68:08:29.8	>27.1	23.53	21.78	20.94
37	17:51:24.96	68:08:33.7	>27.1	22.69	21.51	20.70
38	17:49:14.64	68:09:10.1	>27.1	22.80	21.14	20.29
39	17:49:08.40	68:09:12.6	>27.1	22.95	21.62	20.38
40	17:48:50.64	68:09:53.3	>27.1	23.23	21.20	20.59
41	17:49:46.80	68:11:01.7	>27.1	23.56	21.75	21.12
42	17:50:17.52	68:11:20.1	>27.1	23.80	21.95	21.20
43	17:48:48.23	68:11:30.8	>27.1	20.56	19.37	18.57
44	17:48:53.52	68:11:47.1	>27.1	23.43	21.59	20.93
45	17:49:08.87	68:11:48.5	>27.1	22.81	21.63	20.77
46	17:51:53.76	68:12:02.5	>27.1	23.88	60.86	21.69
47	17:49:8.16	68:12:18.4	>27.1	22.87	21.24	20.56
48	17:49:6.24	68:12:28.1	>27.1	22.25	20.96	20.14
49	17:49:7.92	68:12:38.9	>27.1	23.82	21.41	20.92
50	17:50:18.72	68:13:32.2	>27.1	23.49	22.18	21.03
51	17:51:42.24	68:13:40.1	>27.1	23.91	21.51	20.99
52	17:49:40.32	68:14:17.2	>27.1	23.94	22.02	21.41
53	17:50:53.52	68:14:39.5	>27.1	21.91	20.97	20.17
54	17:49:59.04	68:14:35.2	>27.1	22.70	21.21	20.49
55	17:49:07.92	68:14:43.8	>27.1	24.21	22.36	21.04
56	17:52:06.72	68:15:00.4	>27.1	23.30	21.11	20.91
57	17:51:12.00	68:15:07.6	>27.1	22.94	20.98	20.43
58	17:52:10.32	68:15:21.2	>27.1	21.95	20.51	19.74
59	17:49:55.68	68:16:18.5	>27.1	23.12	21.69	20.88
60	17:50:04.80	68:16:25.7	>27.1	22.90	21.45	20.63
61	17:49:57.37	68:16:37.9	>27.1	22.92	21.47	20.60
62	17:50:43.20	68:16:52.3	>27.1	21.61	20.86	19.92
63	17:50:57.84	68:16:50.5	>27.1	24.32	22.01	21.12
64	17:51:59.76	68:18:07.6	>27.1	22.84	21.36	20.59
65	17:49:59.76	67:58:59.5	>27.1	24.38	22.23	21.42

Table 6. continued.

ID	RA	Dec.	B	z	J	Ks
66	17:50:49.92	68:01:34.3	>27.1	22.91	21.27	20.39
67	17:51:24.72	68:01:41.9	>27.1	23.38	21.41	20.17
68	17:51:19.44	68:03:00.0	>27.1	23.79	21.87	20.74
69	17:51:30.48	68:03:27.4	>27.1	23.35	21.46	20.57
70	17:51:40.32	68:03:37.1	>27.1	23.81	22.06	20.96
71	17:49:20.64	68:04:45.8	>27.1	23.38	21.49	20.50
72	17:50:47.52	68:05:13.9	>27.1	23.70	22.34	20.82
73	17:52:06.96	68:06:02.9	>27.1	18.65	60.86	16.64
74	17:52:10.08	68:06:22.0	>27.1	18.43	60.86	16.13
75	17:48:54.00	68:07:07.3	>27.1	19.29	60.86	16.74
76	17:50:38.40	68:07:05.9	>27.1	24.09	21.95	21.26
77	17:49:56.88	68:07:07.7	>27.1	24.29	22.79	21.27
78	17:52:05.75	68:07:12.4	>27.1	24.28	22.03	20.88
79	17:49:41.04	68:07:18.1	>27.1	23.47	21.69	20.97
80	17:50:23.28	68:07:29.3	>27.1	23.53	21.94	20.76
81	17:49:43.92	68:07:54.1	>27.1	23.74	21.90	21.21
82	17:51:15.60	68:08:19.0	>27.1	24.08	22.32	21.41
83	17:50:48.96	68:08:24.7	>27.1	23.21	20.80	20.48
84	17:51:40.56	68:08:47.0	>27.1	23.41	21.79	20.77
85	17:49:06.49	68:08:57.1	>27.1	23.07	21.03	20.19
86	17:51:29.51	68:09:00.7	>27.1	23.48	22.13	20.65
87	17:50:32.64	68:09:07.9	>27.1	24.08	21.79	20.92
88	17:49:22.09	68:10:08.0	>27.1	23.01	21.30	20.35
89	17:51:35.04	68:10:12.4	>27.1	23.73	21.89	21.38
90	17:49:16.80	68:11:15.0	>27.1	22.42	21.14	20.13
91	17:52:28.56	68:12:09.7	>27.1	24.15	21.54	20.70
92	17:51:29.04	68:12:57.6	>27.1	23.37	21.09	20.84
93	17:49:36.48	68:13:08.8	>27.1	23.81	21.36	20.94
94	17:48:56.16	68:13:18.8	>27.1	22.75	21.14	19.94
95	17:48:58.08	68:13:43.7	>27.1	23.67	22.19	20.83
96	17:51:21.36	68:13:49.1	>27.1	23.07	21.53	20.64
97	17:50:05.52	68:14:05.6	>27.1	22.95	21.00	20.57
98	17:49:06.96	68:14:19.3	>27.1	23.11	21.22	20.36
99	17:50:05.04	68:14:22.6	>27.1	23.35	60.86	20.56
100	17:49:13.92	68:14:31.6	>27.1	22.52	60.86	19.85
101	17:51:16.08	68:14:49.2	>27.1	23.81	22.27	20.93
102	17:49:55.92	68:15:12.2	>27.1	23.70	21.68	20.88
103	17:51:12.48	68:15:11.5	>27.1	23.55	21.50	20.79
104	17:51:24.00	68:15:33.8	>27.1	23.80	21.69	21.21
105	17:49:24.72	68:15:47.2	>27.1	23.93	22.54	21.30
106	17:51:49.92	68:17:51.4	>27.1	23.53	60.86	20.53

[b] See Table 5, note a.